© 2020. Published by The Company of Biologists Ltd | Development (2020) 147, dev190298. doi:10.1242/dev.190298

HUMAN DEVELOPMENT

RESEARCH ARTICLE

E2A regulates neural ectoderm fate specification in human embryonic stem cells

Siqi Yi[1,2], Xiaotian Huang[2], Shixin Zhou[2], Yuan Zhou[3], Michele K. Anderson[4], Juan Carlos Zúñiga-Pflücker[4], Qingxian Luan[1,*] and Yang Li[2,*]

ABSTRACT

E protein transcription factors are crucial for many cell fate decisions. However, the roles of E proteins in the germ-layer specification of human embryonic stem cells (hESCs) are poorly understood. We disrupted the *TCF3* gene locus to delete the E protein E2A in hESCs. E2A knockout (KO) hESCs retained key features of pluripotency, but displayed decreased neural ectoderm coupled with enhanced mesoendoderm outcomes. Genome-wide analyses showed that E2A directly regulates neural ectoderm and Nodal pathway genes. Accordingly, inhibition of Nodal or E2A overexpression partially rescued the neural ectoderm defect in E2A KO hESCs. Loss of E2A had little impact on the epigenetic landscape of hESCs, whereas E2A KO neural precursors displayed increased accessibility of the gene locus encoding the Nodal agonist CRIPTO. Double-deletion of both E2A and HEB (*TCF12*) resulted in a more severe neural ectoderm defect. Therefore, this study reveals critical context-dependent functions for E2A in human neural ectoderm fate specification.

KEY WORDS: E2A, Neural differentiation, Nodal signaling pathway, PRC2 complex, Human embryonic stem cells

INTRODUCTION

Human embryonic stem cells (hESCs) can be expanded indefinitely and differentiate into all human cell types (Thomson et al., 1998; Reubinoff et al., 2000). As such, they hold great promise for developmental studies, drug screening, cell-based therapy and disease modeling (Gepstein, 2002). Thus, a deep understanding of the signaling mechanisms governing hESCs differentiation into early cell lineages is of great importance. Significant advances have been made towards the understanding of the growth factors, intracellular pathways and transcriptional regulatory networks involved in regulating self-renewal and differentiation of hESCs (Boyer et al., 2005).

E2A, which is encoded by the *TCF3* gene locus, belongs to the E protein transcription factor family, which also includes HEB (*TCF12*) and E2-2 (*TCF4*). E proteins regulate transcription of their target genes as obligate dimers, dimerizing with each other or with class II basic helix-loop-helix factors (de Pooter and Kee, 2010; Belle and Zhuang, 2014). The functions of E2A have been most extensively studied in the context of mouse lymphopoiesis (Xu et al., 2013; Wohner et al., 2016). E2A$^{-/-}$ (*Tcf3*$^{-/-}$) mice lack B cells in fetal liver, bone marrow and spleen, and are prone to die from lymphomas (Zhuang et al., 1994; Bain et al., 1997). E2A also regulates the differentiation of neurons from neural stem cells in embryonic (E14.5) mice (Fischer et al., 2014). In humans, E2A was reported to play an important role in leukemogenesis (Duque-Afonso et al., 2016; Vagapova et al., 2018). However, far less is known about the function of E2A in cell-fate regulation of hESCs. It is important to distinguish TCF3 from T cell factor 3 (TCF7L1), a member of the TCF/LEF family of transcription factors that is commonly, and erroneously, referred to as TCF3 in the literature.

In early vertebrate embryogenesis, the Nodal signaling pathway, acting through the SMAD2 and SMAD3 transcription factors, is crucial for mesoendoderm development (Schier, 2003; Shen, 2007). In hESCs, the Nodal signaling pathway has been shown to maintain pluripotency through complex interactions with pluripotency factors, including Nanog (Vallier et al., 2009). The overexpression of Nodal in hESCs can block the default neural ectoderm differentiation during the formation of embryoid bodies (EBs) (Vallier et al., 2004). In mouse embryonic stem cells (mESCs) undergoing mesoendoderm differentiation, HEB forms a complex with SMAD2 and SMAD3 to replace HEB and/or polycomb repressor complex 2 (PRC2) at mesoendoderm gene loci. Furthermore, HEB knockdown promotes mesoendoderm differentiation (Yoon et al., 2015). In contrast, HEB deficiency in hESCs has a profoundly negative impact on mesoderm formation, with HEB directly regulating genes in the Nodal signaling pathway (Li et al., 2017). E2A is a required cofactor for Nodal signaling in mesoendoderm specification, as *Xenopus* embryos depleted for E2A fail to form mesoderm, have reduced endoderm and fail to gastrulate (Yoon et al., 2011; Wills and Baker, 2015).

In mammalian cells, E2A forms dimers to regulate various biological processes by directly binding the promoters of functional genes (Kee, 2009; Núñez-Enríquez and Mejía-Aranguré, 2015). In T-cell development, E2A collaborates with HEB to suppress the innate lymphoid cell transcription signature by activating the expression of genes associated with Notch receptors, T cell receptor (TCR) assembly and TCR-mediated signaling (Miyazaki et al., 2017). Similarly, genetic depletion of E2A splice variant E47 increased the number of Tbr1^{+} deep layer neurons and Satb2^{+} upper layer neurons at E14.5 through binding to a distal enhancer and activating the expression of the cyclin-dependent kinase inhibitor (CDKI) (Pfurr et al., 2017). Moreover, PRC2-based CpG methylation and H3K27me3 repressive epigenetic marks were preferentially altered in the promoter regions of genes bound by E2A, suggesting they synergistically regulate a drug resistance phenotype in B-cell lymphoma (Flinders et al., 2016). However, the interplay between the Nodal signaling pathway and E2A in mediating hESC differentiation into the three germ layers remains largely unknown.

[1]Department of Periodontology, Peking University School and Hospital of Stomatology, National Engineering Laboratory for Digital and Material Technology of Stomatology, Beijing Key Laboratory of Digital Stomatology, Beijing 100081, China. [2]Department of Cell Biology, School of Basic Medical Sciences, Peking University Stem Cell Research Center, Peking University, Beijing 100191, China. [3]Department of Biomedical Informatics, School of Basic Medical Sciences, Peking University, Beijing 100191, China. [4]Department of Immunology, University of Toronto, Sunnybrook Research Institute, Toronto, ON M4N 3M5, Canada.

*Authors for correspondence (kqluanqx@126.com; liyang@bjmu.edu.cn)

Q.L., 0000-0003-0209-8622; Y.L., 0000-0002-8805-4980

Handling Editor: Gordon Keller
Received 6 March 2020; Accepted 27 October 2020

Development (2020) 147, dev190298. doi:10.1242/dev.190298

Here, we have investigated the role of E2A in the self-renewal and differentiation of hESCs. E2A-deficient hESCs [E2A knockout (KO) hESCs] were established via CRISPR-Cas9 gene editing methods. Our results demonstrated that although E2A is dispensable for hESC self-renewal, its deficit delays neural ectoderm differentiation and promotes mesoendoderm outcomes. RNA-seq and ChIP-seq experiments revealed E2A directly bound to the promoters of neural ectoderm differentiation genes, as well as the gene encoding the Nodal agonist Cripto (*TDGF1*). Small molecule-mediated inhibition of the Nodal signaling pathway and/or overexpression of E2A in E2A KO hESCs partially or completely rescued the neural ectoderm differentiation defect. Although E2A interacts with the PRC2 complex, loss of E2A did not lead to changes in the genome-wide distribution of H3K27me3 and H3K4me3 in neural ectodermal lineages. In addition, E2A loss of function did not appear to change the distribution of H3K27me3 and H3K4me3 near the promoters of genes associated with neural ectoderm. Of note, loss of E2A decreased H3K27me3 and increased H3K4me3 near the promoter of the gene encoding Cripto at day 3 after neural differentiation. Last, we demonstrated that $E2A^{KO}$ HEB^{KO} double-deficient hESCs exhibited a more severe neural differentiation defect. Taken together, this study reveals a crucial context-dependent function and mechanism for E2A in regulating neural ectoderm fate specification in hESCs.

RESULTS

E2A is dispensable for the maintenance of hESC pluripotency

To evaluate the role of E2A in hESC pluripotency maintenance and differentiation, we generated E2A-deficient (E2A KO) hESCs by deleting several nucleotides in the first exon of *TCF3* using CRISPR/Cas9 guided gene editing. After sorting and expanding, we identified two clones containing unique deletion mutations (KO-1 and KO-4) (Fig. S1A,B). Western blot analysis demonstrated the absence of E2A protein in KO-1 and KO-4 clones (Fig. S1C,D). We selected E2A KO-1 and KO-4 as our primary models for further analysis.

To assess whether E2A KO hESCs maintain their pluripotent stem cell characteristics, we evaluated colony morphology, growth rate and gene expression. Colony morphology was indistinguishable between wild-type and E2A KO hESCs (Fig. 1A). We also employed colony-forming assay to assess the morphology. The colony-forming assay results demonstrated that wild-type and E2A KO hESCs exhibited similar colony morphology. However, E2A KO group exhibited more colonies after 7 days of culture, which indicates a higher proliferation rate in E2A KO group (Fig. S2A). Consistent with the colony-forming results, the CCK8 assay results revealed that E2A KO hESCs displayed a higher proliferation rate compared with the wild-type group (Fig. 1B). We employed immunofluorescence staining to assess pluripotent marker expression. The wild-type and E2A KO hESCs demonstrated indistinguishable expression levels of OCT4, NANOG, SOX2, SSEA4, TRA-1-60 and TRA-1-81 (Fig. 1C). Western blot analysis also revealed that the loss of E2A did not alter the expression levels of the pluripotent markers OCT4, NANOG and SOX2 (Fig. 1D,E). Given that E2A belongs to bHLH family members, which could regulate cell differentiation via Nodal signaling pathway (Rao et al., 2020), we also assessed the expression level of SMAD2 and p-SMAD2 in wild-type and E2A KO hESCs. The western blot analysis demonstrated significantly decreased p-SMAD2 expression in the E2A KO group and relatively similar SMAD2 expression levels between the wild-type and E2A KO groups (Fig. S2B). To examine the effects of E2A loss on hESC differentiation, we used teratoma formation and directional differentiation models. We injected wild-type and E2A KO hESCs into immunocompromised (NOD-SCID) mice to allow for teratoma development (Fig. 1F). The immunohistochemistry histological analysis revealed that the E2A KO group exhibited increased expression level of mesendodermal markers α-SMA and pan-CK, and decreased expression level of neural differentiation markers β-III-tubulin compared with the wild-type group (Fig. 1G), indicating potentially promoting and inhibitory roles of E2A in hESC mesendodermal differentiation and neural specification, respectively.

Global transcriptome analysis of wild-type and E2A KO hESCs

To examine the impact of E2A absence on the hESC transcriptome, we performed RNA-seq analyses of wild-type and E2A KO hESCs. We found no perturbations in the expression of key pluripotency genes, including OCT4 and NANOG, further demonstrating that E2A is dispensable for hESC self-renewal (Fig. 2A, Table S3). Additionally, principal component analysis (PCA) and a global gene expression heatmap demonstrated that few gene clusters were differentially expressed between wild-type and E2A KO hESCs (Fig. 2B,C). However, we found that E2A KO hESCs demonstrated significantly increased mesoderm and endoderm genes, and decreased neural ectoderm genes, revealing a mesoendoderm bias in E2A KO hESCs at the transcriptome level (Fig. 2D).

Analysis of E2A direct binding to neural ectoderm gene loci

In order to reveal the mechanism by which E2A influences mesoendoderm gene expression, we performed E2A ChIP-seq. The E2A target peaks were mainly distributed in intronic and distal intergenic regions (Fig. 2E, Table S4). We observed that E2A target genes were principally related to neural differentiation, nervous system development and neurogenesis (Fig. 2F, Table S5). We then combined the results from RNA-seq and ChIP-seq analyses, and observed that expression of no genes was significantly increased and expression of 10 genes was decreased in the absence of E2A (Fig. 2G). Moreover, we found that E2A can directly bind to the promoters and gene body regions of the early neural differentiation genes, such as *SOX5* and *FGF1* (Fig. 2H). Thus, our results suggested that there was a potential disruption in the priming for neural ectoderm gene expression in hESCs lacking E2A.

E2A absence promotes mesoendoderm differentiation of hESCs

To evaluate how E2A absence impacted mesoendoderm differentiation, we induced differentiation of wild-type and E2A KO hESCs into definitive endoderm precursors and mesodermal cells (Takayama and Mizuguchi, 2017). First, expression of definitive endoderm precursors were induced by timed exposure to Wnt3A, BMP4, activin A and bFGF (Fig. 3A). After 4 days, cultures were dissociated and stained for CD117, CD184, FOXA2 and SOX17, all of which mark definitive endoderm lineage cells (Fig. 3A). As expected, a robust population of $CD117^{+}$ $CD184^{+}$ double-positive cells developed in the wild-type cultures. However, this population was increased in E2A KO hESC-derived cultures. $FOXA2^{+}SOX17^{+}$ double-positive cells were also present in the wild-type cultures and this population was significantly increased in the absence of E2A (Fig. 3C,D). Next, we induced differentiation of blood cells using a canonical protocol (Li et al., 2017) (Fig. 3B). At day 4 of culture, early mesoderm and endoderm lineage marker genes were increased in E2A KO hESCs (Fig. 3G), consistent with enhanced mesodermal differentiation. Furthermore, by day 8 of

Development (2020) 147, dev190298. doi:10.1242/dev.190298

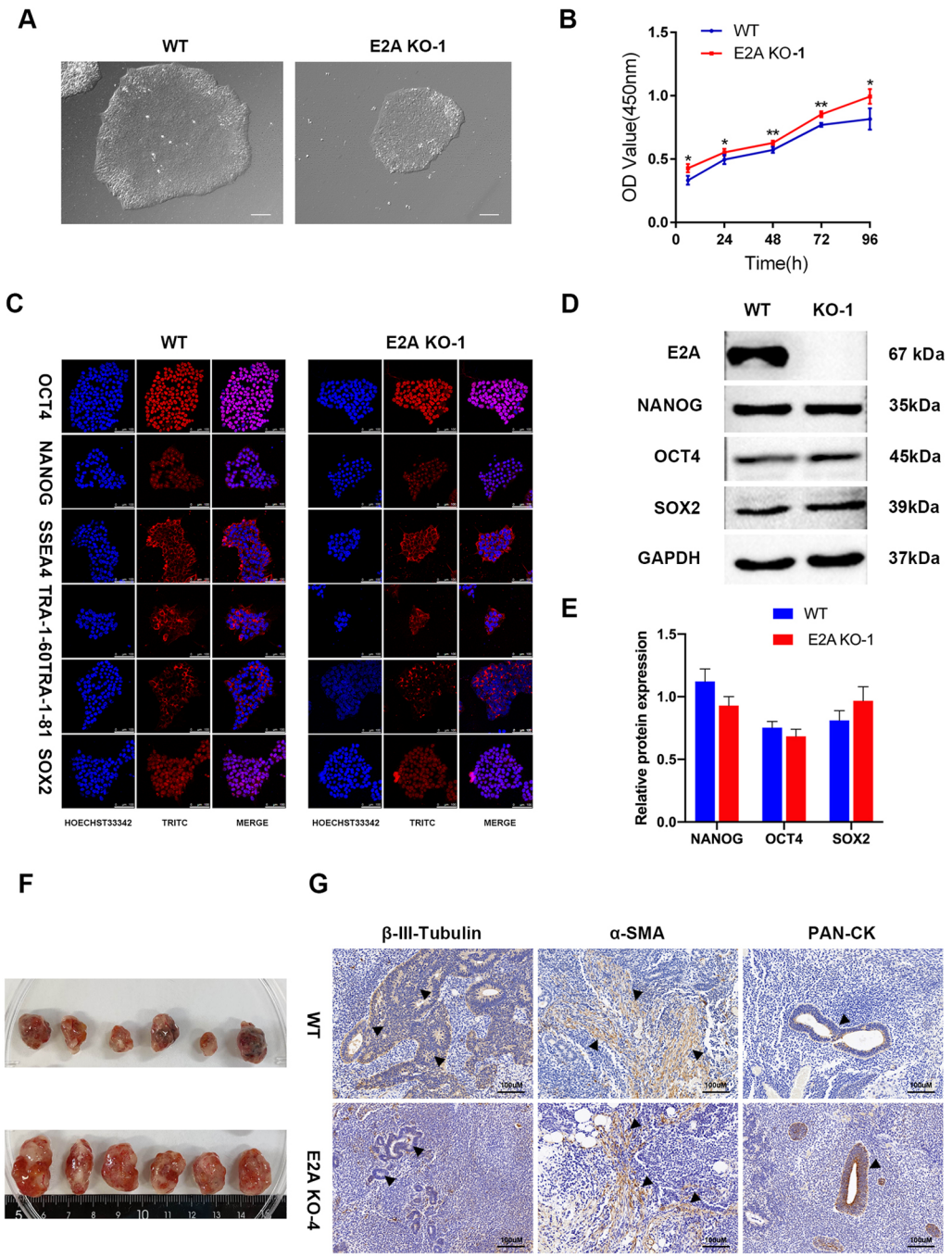

Fig. 1. Comparison of the pluripotency features of wild-type and E2A KO hESCs. (A) Morphology of wild-type and E2A KO hESCs (representative images of morphology are irrelevant to proliferation). (B) CCK8 analysis of proliferation rate in wild-type and E2A KO hESCs. (C) Immunofluorescence analysis of OCT4, NANOG, SSEA4, TRA-1-60, TRA-1-81 and SOX2 in wild-type and E2A KO hESCs. (D) Western blot analysis of E2A, OCT4, NANOG, SOX2 and GAPDH in wild-type and E2A KO hESCs. (E) Quantitative analysis of OCT4, NANOG and SOX2 expression level using Image J software. (F) Teratomas collected from six mice per hESC genotype. (G) Representative immunohistochemistry staining for ectoderm (β-III-tubulin), mesoderm (α-SMA) and endoderm (pan-CK) of teratomas formed in wild-type and E2A KO hESCs. Arrows indicate distinguishing features of each tissue type. Images in A,C,D,G are representative of three independent experiments. Data are mean±s.d. (n=3 independent experiments). *P<0.05, **P<0.01 (Student's t-test). Scale bars: 100 µm in A,C,G.

culture a higher percentage of $CD34^+$ hematopoietic progenitor cells was present in E2A KO when compared with wild-type cultures (Fig. 3E,F). Taken together, our data demonstrate that loss of E2A promotes differentiation of mesoendoderm from hESCs.

E2A loss of function delays hESC neural ectoderm differentiation

In order to investigate the function of E2A during neural differentiation of hESCs, we next examined the expression levels of early neural lineage marker genes in teratomas formed from wild-type and E2A KO hESCs. Immunohistochemistry staining demonstrated higher expression levels of NES (nestin) and SOX1 in wild type, mainly in the rosette region, compared with E2A KO teratomas (Fig. 4A). We then induced hESCs to differentiate towards a neural fate using commercial medium that could drive rapid neural differentiation in hESC (Saini et al., 2017). We observed that E2A expression exhibited a decrease in the first 2 days of induction, whereas it gradually increased afterwards (Fig. S3A,B). We also stained for the expression of SOX1 and PAX6, which mark neural progenitor cells. After 6 days and 9 days of neural induction, a large fraction of the wild-type cells were $SOX1^+PAX6^+$, while fewer $SOX1^+PAX6^+$ cells were present in E2A KO cultures (Fig. 4B,C, Fig. S3C), indicating a significant delay in early neural differentiation. Moreover, we also generated E2A KO cells with the same CRIPSR/Cas 9 plasmid in H9 cell line (Fig. S5A,B). Consistently, the E2A KO H9 clones exhibited significantly decreased SOX1 and PAX6 expression compared with wild-type H9 cells (Fig. S5C). To monitor the dynamic changes of gene expression during neural

Development (2020) 147, dev190298. doi:10.1242/dev.190298

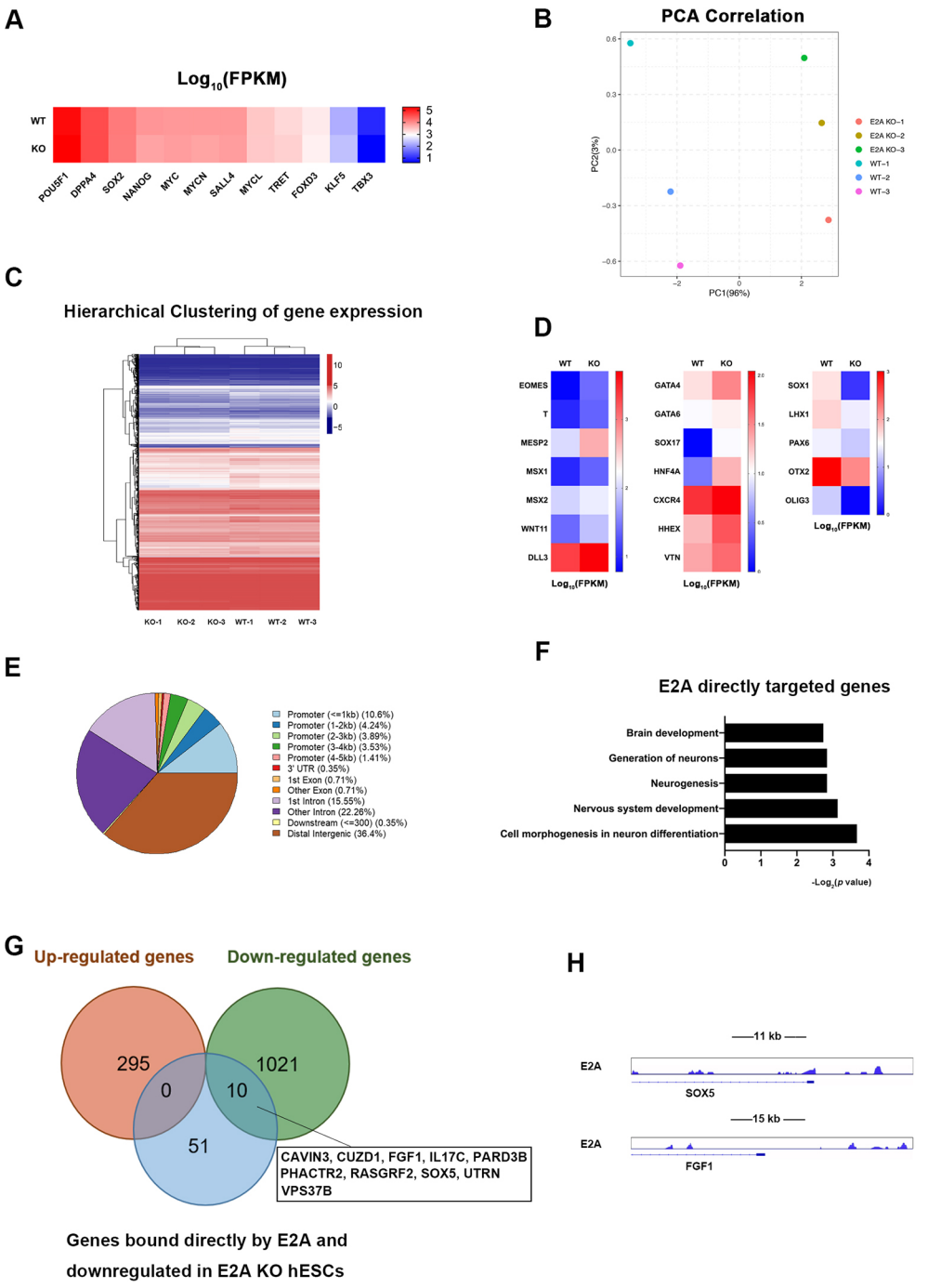

Fig. 2. Global transcriptome analysis of wild-type versus E2A KO hESCs. (A) Heatmap illustrating the RNA expression in wild-type and E2A KO hESCs of RNA-seq analysis for selected genes of pluripotency. FPKM, fragments per kilobase of transcript per million mapped reads. (B) The PCA correlation heatmap between wild-type and E2A KO hESCs. (C) The global transcriptome analysis of wild-type and E2A KO hESCs. (D) Heatmap illustrating the RNA expression in wild-type and E2A KO hESCs of RNA-seq analysis for selected genes of different lineages. (E) ChIP-seq E2A-binding regions were mapped relative to their nearest downstream genes. Color indicates whether a peak is in the promoter, 3′ UTR, 1st exon, other exon or intron, etc. (F) GO functional clustering of genes allows for identification of cellular functions directly regulated by E2A. (G) Overlap of RNA-seq and ChIP-seq results revealed 10 genes as potential direct targets of E2A in wild-type hESCs. (H) The binding of E2A to the representative E2A target genes *SOX5* and *FGF1* in hESCs.

differentiation of E2A KO hESCs, we performed RNA-seq analysis on wild-type and E2A KO cultures after a 3-day neural induction. RNA-seq data indicated a more substantial change in global gene expression than that seen in undifferentiated hESCs (Fig. 4E), with 3347 genes upregulated and 2009 genes downregulated in E2A KO cells after neural differentiation (Table S6). Furthermore, heatmaps of Pearson values and differential gene expression demonstrated a closer relationship between KO-1 and KO-4, than between the wild type and both E2A KOs (Fig. 4D,E). Gene ontology (GO) analysis revealed that the downregulated genes were enriched for neural ectoderm markers and were mainly involved in nervous system development (Fig. 4F). In addition, qPCR analysis showed that E2A KO cells had significantly lower levels of the early neural markers PAX6 and NES, while retaining higher levels of the pluripotency markers OCT4 and NANOG, when compared with wild-type cells (Fig. 4G). Consistent with the qPCR analysis, the western blot analysis demonstrated higher levels of pluripotency markers OCT4 and NANOG in the E2A KO group (Fig. S4A). Moreover, the immunofluorescence analysis also exhibited higher expression levels of OCT4 in the E2A KO group (Fig. S4B). Considering the counterbalance of proliferation and differentiation (Singh and Hansen, 2017), we employed EdU staining to further ascertain the role of E2A in neural differentiation. The EdU results revealed a lower proliferation rate of the E2A KO group in the neural induction period, which is contrary to hESCs results (Fig. S3D). The data suggest that absence of E2A compromises early neural differentiation from hESCs.

Development (2020) 147, dev190298. doi:10.1242/dev.190298

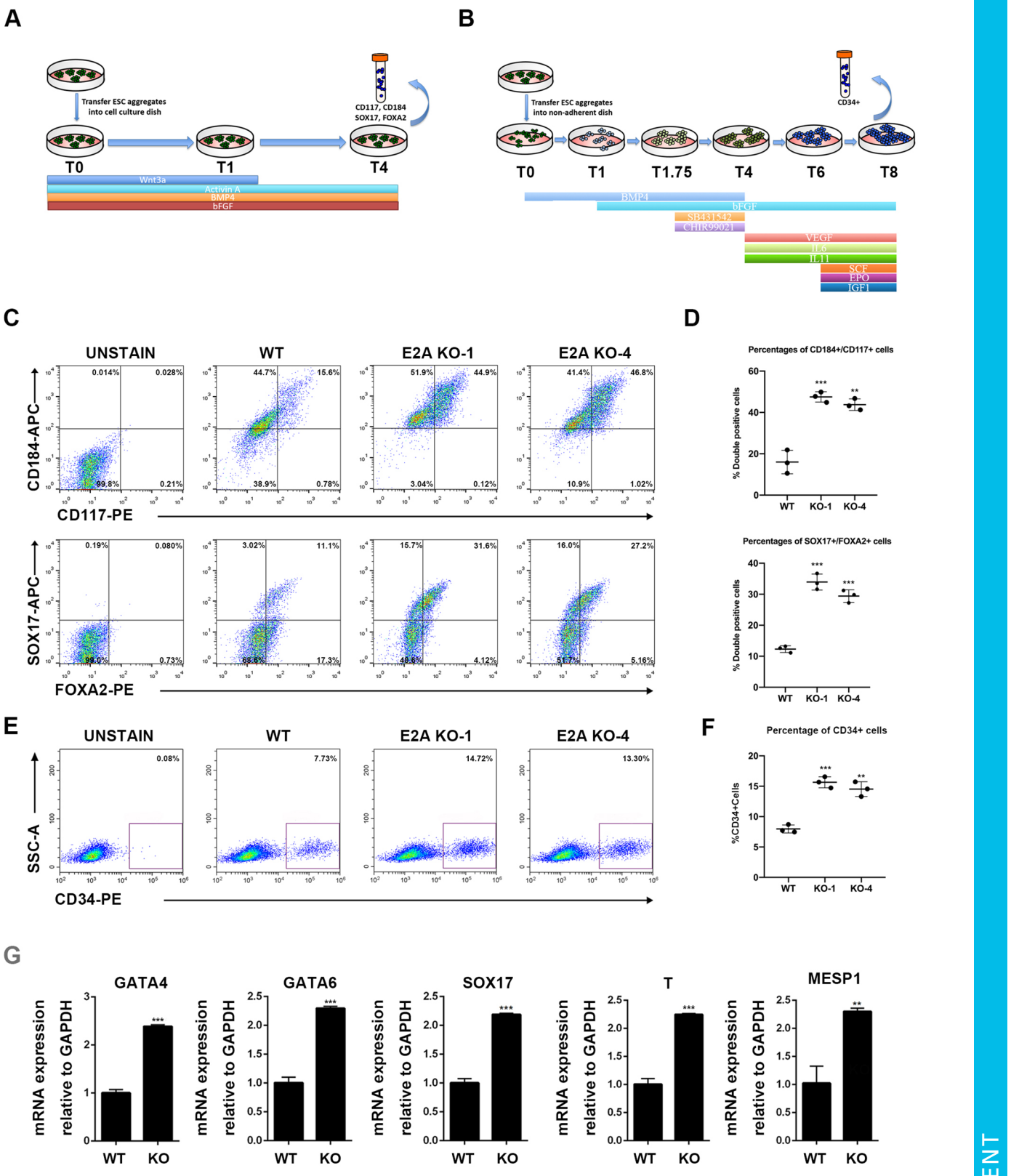

Fig. 3. E2A depletion promotes mesoendoderm differentiation of hESCs. (A,B) Experimental overviews of (A) non-embryoid body (EB) formation and differentiation into definitive endoderm (DE), and (B) embryoid body (EB) formation and differentiation into hematopoietic precursor. BMP4, bone morphogenetic protein 4; bFGF, basic fibroblast growth factor; VEGF, vascular endothelial growth factor; IL, interleukin; SCF, stem cell factor; FLT3L, FMS-like tyrosine kinase 3 ligand; TPO, thrombopoietin. (C) Flow-cytometric analysis of CD117, CD184, SOX17 and FOXA2 expression in DE differentiated cells on day 4. (D) The percentage of CD117, CD184, SOX17 and FOXA2 expression in DE differentiated cells on day 4. $^{**}P<0.01$, $^{***}P<0.005$ (Student's *t*-test). (E) Flow-cytometric analysis of CD34 expression in hematopoietic precursors on day 8. (F) The percentage of $CD34^{+}$ cells in day 8 EBs. $^{**}P<0.01$, $^{***}P<0.005$ (Student's *t*-test). (G) qRT-PCR analysis of the expression of endoderm and mesodermal genes in day 4 DE (GATA4, GATA6, SOX17) and EB (T, MESP1) differentiation cells. $^{**}P<0.01$, $^{***}P<0.005$. Images in C and E are representative of three independent experiments. Data are mean±s.d. (n=3 independent experiments).

Development (2020) 147, dev190298. doi:10.1242/dev.190298

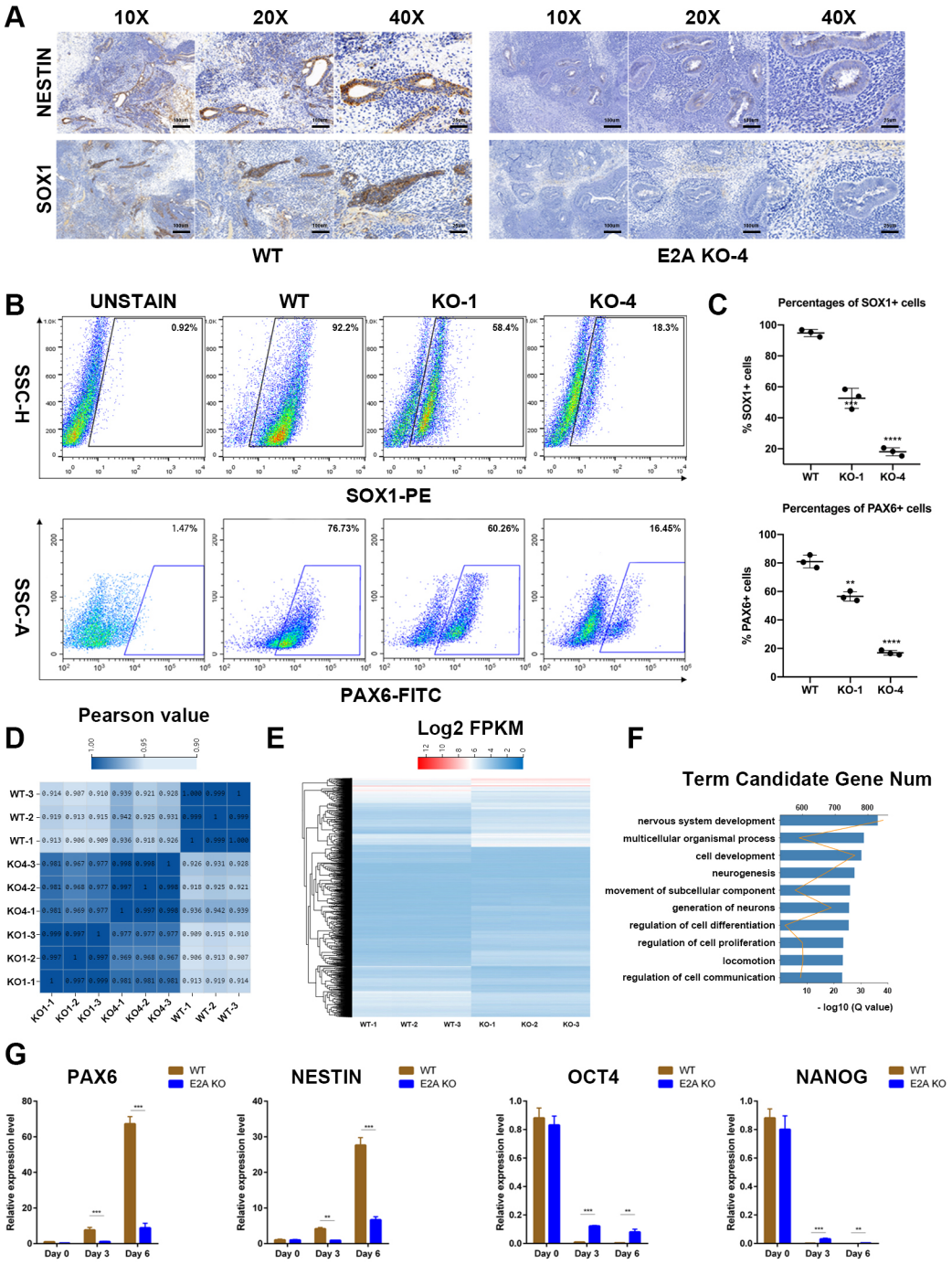

Fig. 4. E2A loss of function delays hESC neural ectoderm differentiation. (A) The immunohistochemistry analysis of NES and SOX1 expression in teratomas formed in wild-type and E2A KO hESCs. (B) Flow-cytometric analysis of SOX1 and PAX6 expression on day 6 neural differentiated cells. (C) The percentage of SOX1^{+} and PAX6 $^{+}$ cells on day6. ***P*<0.01, *****P*<0.0001 (Student's *t*-test). (D) The Pearson rank correlation analysis on the whole-genome transcriptome of wild-type, E2A KO-1 and E2A KO-4 hESCs after neural differentiation. (E) The global transcriptome analysis of wild-type, E2A KO-1 and E2A KO-4 hESC after 3 days of neural differentiation. (F) GO functional clustering numbers of different expression genes allow the identification of cellular functions. (G) qRT-PCR analysis for expression of pluripotency and differentiation markers in undifferentiated hESCs (day 0), day 3 neural differentiated cells (wild-type and E2A KO-1 hESCs) and day 6 neural differentiation cells (wild-type and E2A KO-1 hESCs). ***P*<0.01, ****P*<0.005 (Student's *t*-test). Images in A are representative of three independent experiments. Data are mean±s.d. (*n*=3 independent experiments).

To investigate whether ectopic expression of E2A can rescue the E2A KO early neural defect, we established cell lines stably expressing E2A in E2A KO hESCs via lentiviral transduction (Lv-E2A). We then induced neural differentiation of wild-type, E2A KO and Lv-E2A (~99% GFP^{+}) hESCs, and western blot analysis demonstrated that restored expression of E2A in E2A KO hESCs rescued the downregulation of PAX6 (Fig. S6A,B). In addition, flow cytometry and qPCR analyses of neural progenitor markers SOX1, PAX6 and NES indicated that E2A restoration rescued the neural differentiation defects (Fig. S6C,D). Overall, E2A overexpression can rescue the neural differentiation defect phenotype of E2A KO hESCs, confirming that the defect was not an off-target effect of gene editing.

Development (2020) 147, dev190298. doi:10.1242/dev.190298

E2A can directly bind to genes involved in neural differentiation

To explore the mechanism leading to the neural differentiation defects, we performed E2A ChIP-seq on day 3 cultures after neural induction in wild-type hESCs. E2A target genes are mainly located in intron, distal intergenic and promoter regions (Fig. 5A, Table S7). Combined with RNA-seq data from day 3 cultures after neural induction, we found 57 genes were significantly upregulated and 29 genes were significantly downregulated, as displayed in a heatmap of differentially expressed genes (Fig. 5B,C). Gene ontology (GO) analysis revealed the downregulated genes were enriched for neural ectoderm markers and mainly involved in central nervous system development, neurogenesis and nervous system development. Furthermore, the upregulated genes were mainly involved in the

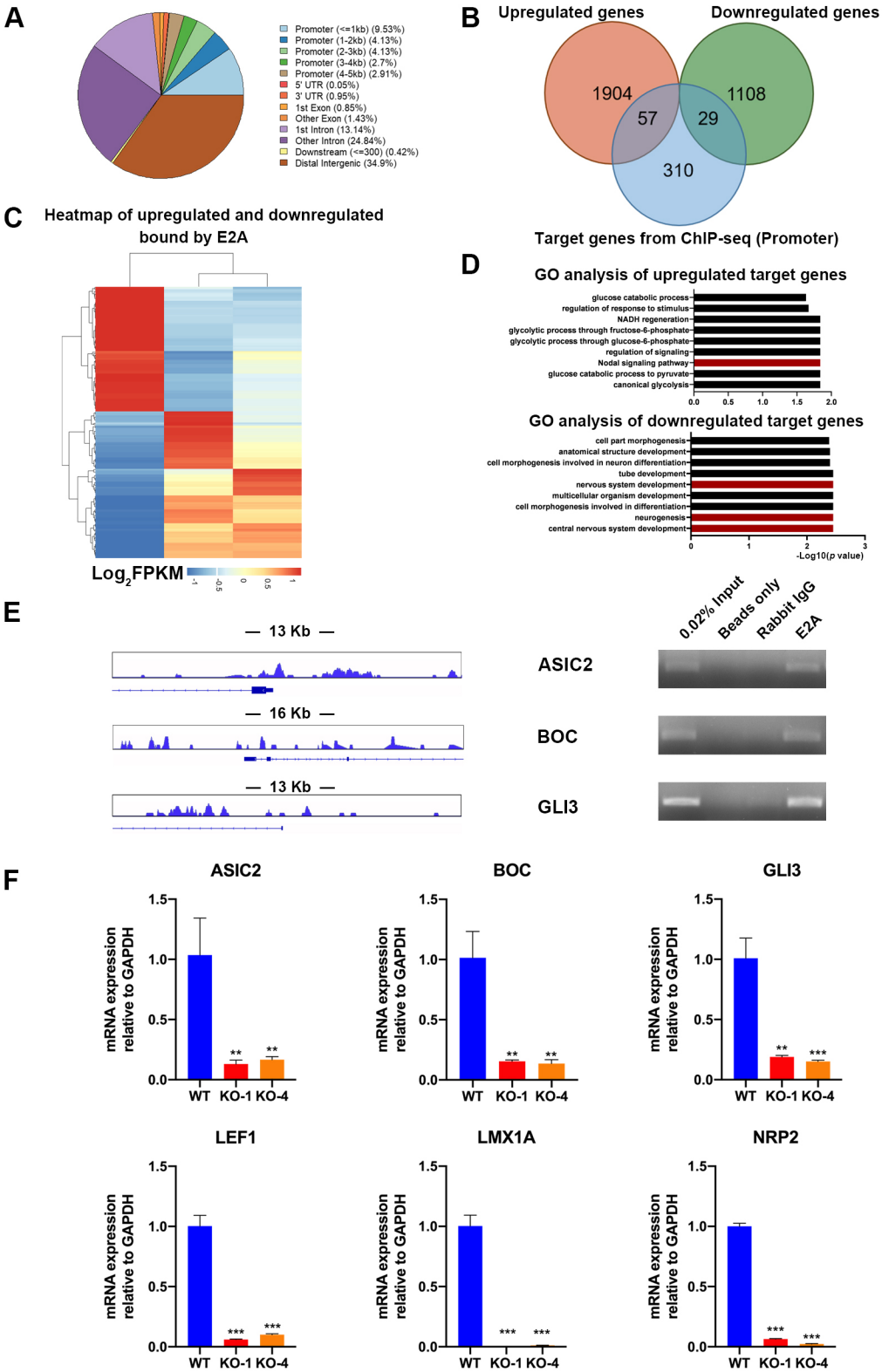

Fig. 5. E2A can directly bind to neural differentiation markers. (A) ChIP-seq E2A-binding regions were mapped relative to their nearest downstream genes. Color indicates whether a peak is in the promoter, 3′UTR, 1st exon, other exon or intron, etc. (B) Overlap of RNA-seq and ChIP-seq results revealed 86 genes as potential direct targets of E2A in wild-type hESCs. (C) Heatmap of E2A target differentially expressed genes in day 3 wild-type neural differentiated cells. (D) GO functional clustering of genes allowed for identification of cellular functions directly regulated by E2A (top 10 categories are shown). (E) The ChIP-seq and ChIP-PCR analysis of E2A binding on representative target genes *ASIC2*, *BOC* and *GLI3* in day 3 neural differentiated cells (the original uncropped image is shown in Fig. S10). (F) qPCR analysis of E2A target genes associated with neural differentiation after 3 days of neural differentiation. Images in E are representative of three independent experiments. Data are mean±s.d. (n=3 independent experiments). $^{**}P$<0.01 $^{***}P$<0.005 (Student's t-test).

Development (2020) 147, dev190298. doi:10.1242/dev.190298

NODAL signaling pathway, which also correlated with neural differentiation (Fig. 5D, Table S8). We found that E2A directly bound to the promoters regions of neural differentiation markers ASIC2, BOC and GLI3 (Fig. 5E, Fig. S10). We also found a striking decrease in expression of these genes, including *ASIC2*, *BOC*, *GLI3*, *LEF1*, *LMX1A* and *NRP2* (Fig. 5F).

Heatmap analysis confirmed that the lack of E2A during neural differentiation led to significantly higher expression of selected Nodal related genes (Fig. S7A,B).

Western blot analysis also demonstrated a higher level of NODAL signaling pathway component p-SMAD2 in E2A KO group (Fig. S4A). Moreover, examination of ChIP-seq data confirmed that E2A loss of function increases the active H3K4me3 marks and decreases the repressive H3K27me3 marks near the promoter of the Nodal agonist CRIPTO, at day 3 of neural differentiation (Fig. S7C). To investigate whether inhibition of the Nodal signaling pathway can rescue the phenotype of the neural differentiation defect, we performed flow cytometry to examine the expression of SOX1 and PAX6 in wild-type and E2A KO hESCs with or without various concentrations (10 µM, 20 µM and 50 µM) of SB431542 treatment. Our data demonstrated that treatment of E2A KO hESCs with 10 µM SB431542 partially rescued the expression of SOX1 and PAX6 caused by E2A loss of function (Fig. S7D). Higher concentration of SB431542 led to a decrease of SOX1 and PAX6 expression in the wild-type group, but could also partially rescue the expression of SOX1 and PAX6 caused by E2A loss of function (Fig. S7D). These data suggest that increased NODAL signaling in the absence of E2A may lead to a defect in neural ectoderm differentiation.

E2A can interact with PRC2 in the neural induction period but does not participate in transcriptional regulation of neural differentiation genes

Given the known interplay between HEB and the PRC2 complex, we subjected the combined RNA-seq and ChIP-seq data to an analysis using the mSigDB database. The downregulated genes were strongly relevant to PRC2 regulation in hESCs, while the upregulated genes were related to EED gene targets in hESCs (Fig. 6A). We next examined the global levels of inhibitory H3K27me3 and activating H3K4me3 marks in cells after 3 days of neural differentiation by western blot analysis. We observed a significant decrease in H3K27me, H3K4me3 and EZH2 levels in E2A KO, HEB KO and E2A HEB double knockout (DKO), compared with wild-type neural differentiated cells (Fig. 6B, Fig. S8). In addition, the immunofluorescence staining of E2A and H3K27me3 in neural differentiated cells demonstrated co-localization between these proteins (Fig. 6C).

To determine whether E2A interacts with H3K27me3 along with PRC2, we performed co-immunoprecipitation (IP) experiments. IP of proteins from neural differentiated cells using anti-E2A, followed by western blot with antibodies against EZH1, EZH2, SUZ12, H3K27me3 and H3K4me3, showed that E2A associated with all of the PRC2 components tested, as well as with methylated H3 (Fig. 6D). Furthermore, IP of proteins from neural differentiated cells using antibodies against EZH1, EZH2, SUZ12, AEBP2 and JARID2, followed by western blot with anti-E2A, confirmed E2A association with EZH1, EZH2 and SUZ12, and showed that E2A also associates with AEBP2 and JARID2 (Fig. 6E). In order to investigate whether E2A regulates the genome-wide distribution of H3K4me3 and H3K27me3 during neural differentiation, we performed ChIP-seq using H3K4me3 and H3K27me3 antibodies in both wild-type and E2A KO neural differentiated cells (at day 3 of neural differentiation). Initial analysis indicated that loss of E2A did not result in major changes in the genome-wide distribution of H3K4me3 and H3K27me3 epigenetic marks (Fig. 6F, Tables S9, S10). After deeper analysis, we found a number of differences in the binding peaks between these groups (see Tables S9, S10). Moreover, after carefully looking into the epigenetic modifications of E2A target genes, including *ASIC2* and *GLI3*, we did not find significantly obvious differences in binding distribution of H3K4me3 and H3K27me3 between wild-type and E2A KO neural differentiated cells (Fig. 6G). Taken together, our data suggest that although E2A can bind to PRC2, its presence does not significantly change the H3K4me3 and H3K27me3 distributions in cells differentiating from wild-type and E2A KO hESCs.

E2A HEB double knockout (DKO) hESCs display a more severe neural differentiation defect

In order to verify whether HEB collaborates with E2A to influence neural differentiation, we generated E2A HEB double knockout (DKO) hESCs using HEB KO hESCs (Fig. S9A). Western blot analysis demonstrated that the DKO hESCs did not express E2A or HEB proteins (Fig. 7A). Furthermore, like E2A KO hESCs, DKO hESCs displayed similar colony morphology to wild type (Fig. 7B). To assess the ability of DKO hESCs to generate neural progenitor cells, day 3 cells were dissociated and stained for the expression of SOX1 and PAX6. Flow cytometry analysis revealed DKO hESCs exhibited fewer $SOX1^+$ and $PAX6^+$ cells when compared with wild-type, E2A KO and HEB KO hESCs (Fig. 7C,D). In addition, immunofluorescence staining indicated DKO hESCs had less expression of PAX6 and NES compared with E2A KO and HEB KO hESCs (Fig. 7E, Fig. S9B). This pattern was mirrored by mRNA expression, as NES and PAX6 failed to be upregulated, while the OCT4 showed opposite behavior (Fig. 7F). Taken together, DKO hESCs displayed more severe differentiation defects, suggesting that both E2A and HEB participate in the differentiation of neural ectoderm.

DISCUSSION

E proteins are crucial components of many developmental processes, but little is known about how E2A, HEB and E2-2 differentially regulate gene expression, especially in humans. Our generation of E2A KO hESCs has provided a highly informative system for studying the specific role of E2A in early human development processes. Here, we report that the absence of E2A results in a delay in neural ectoderm specification, associated with a failure to upregulate critical neural differentiation genes in hESCs. Furthermore, during development, E2A deficiency can inhibit neural differentiation by directly regulating the expression levels of neural genes. Conversely, we have previously shown that HEB KO hESCs are compromised in their ability to differentiate along the mesoendodermal pathway. Together, these discoveries demonstrate that E2A and HEB provide crucial non-redundant forces in shaping the outcomes of human developmental events, and provide compelling evidence that E2A and HEB can act in opposition to each other in promoting either the neural ectoderm or the mesoendodermal fates.

As with all E protein family members, E2A acts by forming homodimers and heterodimers with other transcription factors that are essential for various biological processes (Jia et al., 2008; Woodcroft et al., 2015). In early *Xenopus* embryo development, E2A can form a complex with HEB, which can associate with SMAD2, SMAD3 and FOXH1, suggesting a crucial role in mesoendoderm specification and gastrulation (Yoon et al., 2011; Wills and Baker, 2015). In our study, we did not observe any significant changes in pluripotency features, reflected by maintenance of pluripotency genes. However, we observed that absence of E2A led to a decline in the expression of the

Development (2020) 147, dev190298. doi:10.1242/dev.190298

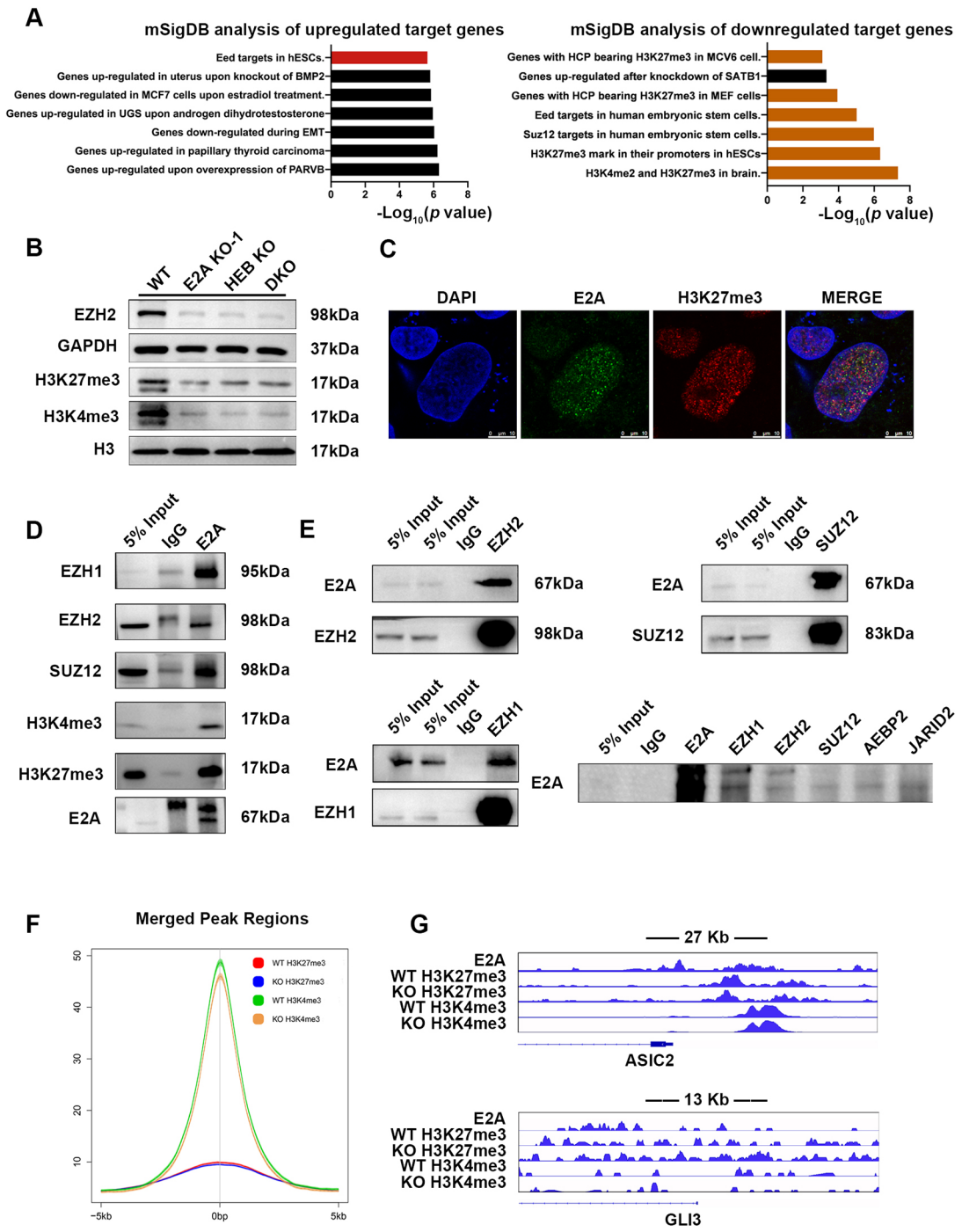

Fig. 6. E2A can interact with PRC2 complex in neural induction period but does not participate in transcription regulation. (A) mSigDB clustering analysis of E2A ChIP-seq allow for identification of cellular functions. (B) Western blot analysis of EZH2, H3K27me3 and H3K4me3 expression in wild-type, E2A KO, HEB KO and E2A KO/HEB KO hESCs after 3 days of neural differentiation. (C) Wild-type neural differentiated cells were immunofluorescently stained for E2A (green) and H3K27m3 (red) expression; nuclei were counterstained with DAPI (blue). (D) E2A was immunoprecipitated from wild-type neural differentiated cells then the amount of EZH1, EZH2, SUZ12, H3K27me3 and H3K4me3 present in the precipitate was evaluated by western blot. (E) EZH1, EHZ2, SUZ12, AEBP2 and JARID2 were immunoprecipitated from wild-type neural differentiated cells, then the amount of E2A present in the precipitate was evaluated via western blot. (F) The merged peak regions of H3K4me3/H3K27me3 in wild-type and E2A KO neural differentiation processes. (G) The binding of E2A, H3K4me3 and H3K27me3 in wild-type and E2A KO hESCs in day 3 neural differentiated cells to the representative target genes *ASIC2* and *GLI3*. Images in B-E are representative of three independent experiments. Scale bars: 10 µm.

neural differentiation genes FGF1 and SOX5. Our observation that E2A binds to the gene body region of these genes suggest that it directly drives their upregulation during neural ectoderm specification. If HEB and E2A acted equivalently, then a decrease in either protein would be expected to result in a similar phenotype. Instead, we found that neural ectoderm differentiation is dependent primarily on E2A, whereas mesoendoderm specification requires HEB. Therefore, our studies suggest that HEB and E2A participate in a balanced circuit that drive fate determination (Thomson et al., 2011; Wang et al., 2012).

Development (2020) 147, dev190298. doi:10.1242/dev.190298

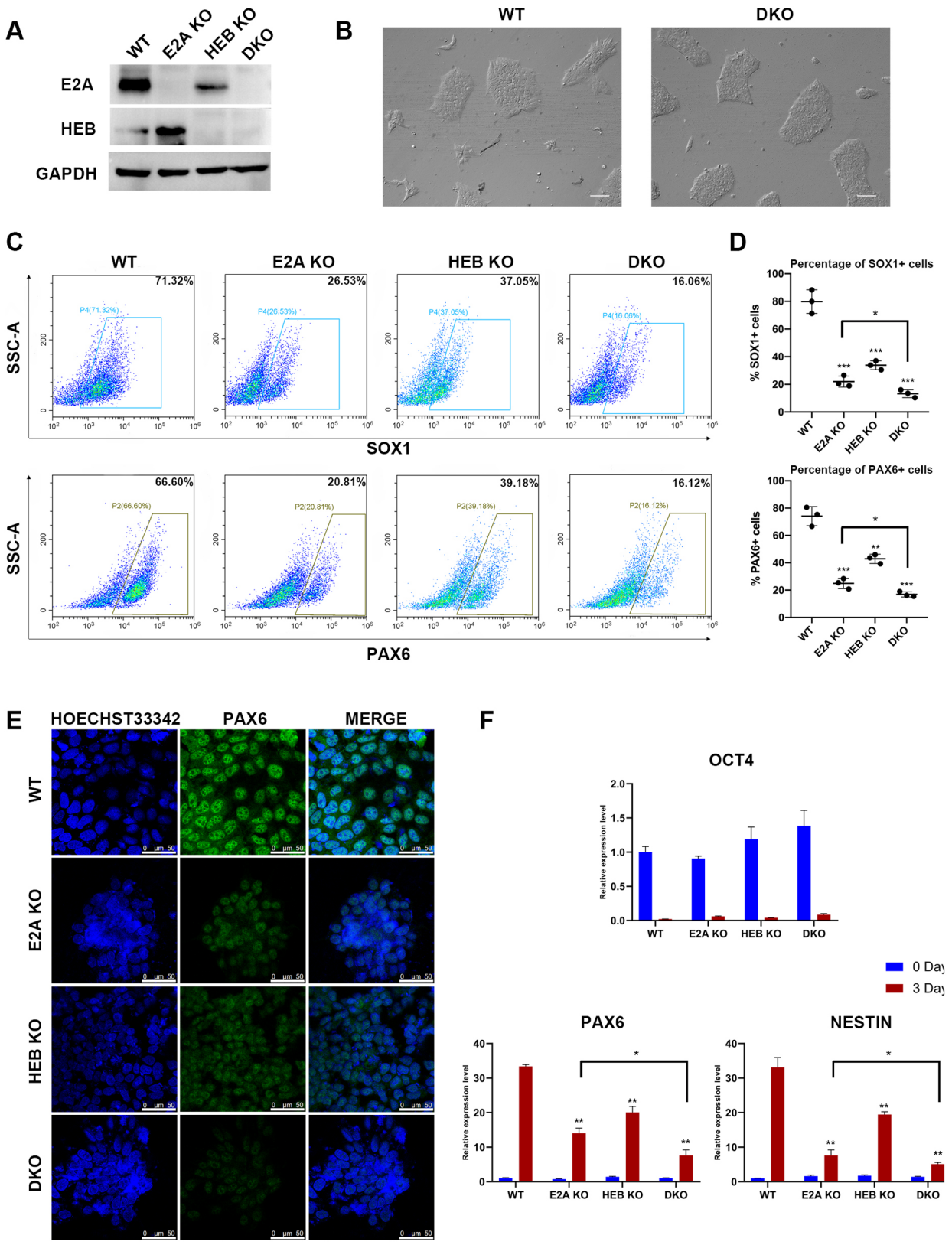

Fig. 7. E2A/HEB double knockout (DKO) hESCs display a more severe neural differentiation defect. (A) Western blot analysis of E2A and HEB expression in wild-type, E2A KO, HEB KO, E2A KO/HEB KO double knockout (DKO) hESCs. (B) The morphology of wild-type and E2A KO/HEB KO double knockout (DKO) hESCs. (C) Flow-cytometric analysis of SOX1 and PAX6 expression on day 3 neural differentiated cells. (D) The percentage of SOX1^{+} and PAX6^{+} cells on d6. *P<0.05, **P< 0.01, ***P<0.005 (Student's t-test). (E) Immunofluorescence analysis of PAX6 in wild-type, E2A KO, HEB KO and E2A KO/HEB KO double knockout (DKO) hESCs after 3 days of neural differentiation. (F) qPCR analysis for expression of pluripotency (OCT4) and differentiation (PAX6 and NES) markers in undifferentiated hESCs (day 0) and in day 3 neural differentiation cells. *P<0.05, **P<0.01 (t-test). Images in A,B,E are representative of three independent experiments. Data are mean±s.d. (n=3 independent experiments). Scale bars: 100 µm in B; 50 µm in E.

Development (2020) 147, dev190298. doi:10.1242/dev.190298

In E2A KO hESCs, the decline of neural differentiation genes is associated with an upregulation of mesoendodermal genes. It remains to be seen whether the mesoendodermal genes are directly or indirectly de-repressed in the absence of E2A. However, we found that the expression of the TGFβ superfamily members NODAL, LEFTY1 and GDF3 was markedly increased in E2A KO hESCs, whereas we have previously shown that they were decreased in HEB KO hESC data (Li et al., 2017). This shift in NODAL pathway gene expression may be another driving force of the mesoendodermal phenotype in the absence of E2A. Therefore, the combination of a failure of induction of neural ectoderm genes and NODAL signaling induction are both involved in the E2A-mediated regulation of early human development.

E2A is known to participate in diverse biological processes using different mechanisms of action. Initially, E2A was reported to play a vital role in hematopoietic differentiation, including promoting the survival of precursor and mature B lymphocytes (Lazorchak et al., 2006; Dias et al., 2008), facilitating T lymphocyte lineage commitment (Xu et al., 2013; Shaw et al., 2016), and promoting the maturation of myelolymphoid and myeloerythroid progenitors (Semerad et al., 2009). In early embryonic development, E2A was reported to participate in mesoendoderm differentiation via regulation of NODAL signaling components (Yoon et al., 2011; Wills and Baker, 2015). One of these components, CRIPTO, sustains hESC self-renewal and is considered to be a driving force in specification of mesoendoderm and neural ectoderm (Parisi et al., 2003; Fiorenzano et al., 2016). In our study, E2A deficiency led to CRIPTO upregulation during neural differentiation, suggesting that E2A regulates NODAL signaling in part by suppressing CRIPTO expression. This occurred in a PRC2-dependent way, revealing a powerful inhibitory role for CRIPTO-mediated NODAL signaling during early germ layer differentiation. Moreover, this finding also provides new insights into the interplay between E2A and NODAL signaling in the regulation of neural ectoderm differentiation.

A crucial role for E2A in neurogenesis is further supported by its widespread expression pattern in the brain. Moreover, it has been shown that E2A manipulation alters the progression of neural differentiation in postnatal SVZ and differentiation of projection neurons during cortical development (Fischer et al., 2014). In our study, we found few genes regulated by E2A in hESCs, whereas a substantial number of targets were observed during neural differentiation, demonstrating that E2A transcription regulation is largely context dependent. The paucity of direct targets of E2A in hESCs, as determined by our ChIP-seq data, strongly contrasts with the ability of HEB to directly bind to gene loci involved mesoendodermal differentiation in hESCs (Li et al., 2017). HEB has also been reported to have broad domains covering the promoters of genes that are significantly enriched for developmental processes, including the Hoxd gene cluster (Yoon et al., 2015). The difference between the target genes of E2A and HEB demonstrates one way in which their absences promote and inhibit mesoendoderm differentiation, respectively. At the same time, we also found E2A deficiency led to severe neural differentiation defect of hESCs due to a failure to directly upregulate expression of neural genes and downregulate expression of Nodal signaling pathway genes. The importance of direct regulation of neural genes by E2A in addition to its impact on NODAL signaling is clear from our finding that E2A-overexpressing lentivirus can completely rescue neural differentiation in E2A KO hESCs, whereas the NODAL inhibitor SB431542 provides only a partial rescue. Therefore, our studies demonstrate dual roles of E2A in regulating hESC neural differentiation: acting as a repressor for the NODAL signaling pathway and functioning as a direct inducer of neural-related genes.

Epigenetic regulation provides another layer of regulation in gene expression by altering chromatin accessibility (Boyer et al., 2006). E proteins have been reported to function closely with the PRC2 complex. In mESCs, HEB can form a complex with PRC2 subunits, leading to inhibition of the expression of the mesodermal-promoting Hoxd gene cluster, thus maintaining the pluripotent state (Yoon et al., 2015). This process was shown to be under tight control of the NODAL signaling pathway. During mesoendodermal differentiation, the HEB/SMAD2/3 complex can replace the HEB/PRC region at mesoendodermal gene loci, which strongly drove mesoendodermal differentiation. Given these results, we infer that the E2A/HEB complex may interact with PRC2 in an environment of low NODAL activity, which corresponds to the cell culture conditions during neural differentiation from hESCs. In addition, it has been shown that PRC2-mediated CpG methylation and H3K27me3 repressive epigenetic markers are preferentially altered in the promoter regions of genes bound by E2A in B cells, suggesting that E2A and PRC2 may act synergistically to protect against the development of B-cell lymphoma (Flinders et al., 2016). We found that E2A could associate with PRC2 subunits EZH1, EHZ2 and SUZ12, and with H3K27me3 during neural differentiation. However, E2A deficiency did not change the distribution H3K27me3 or H3K4me3, indicating that the function of PRC2 is likely independent of E2A in this context. We also found that the absence of E2A led to a decline of EZH2 during neural differentiation. E2A has been reported to take part in ubiquitylation and degradation facilitated by ChIP and Hsc70 in a Notch signaling-dependent manner (Huang et al., 2004). Therefore, the unexpected decline of EZH2 may relate to abnormal ubiquitylation and degradation processes in E2A-deficient cells.

It is known that E2A and HEB synergize to play vital roles in mesoendodermal differentiation (Yoon et al., 2011). However, it has been unclear whether such coordination occurs during neural differentiation. Our generation of E2A KO HEB KO DKO hESCs provided us with a new tool with which to address this issue, enabling us to determine that DKO hESCs display more severe neural differentiation defects than E2A KO cells. This finding clearly demonstrated a collaborative interaction between E2A and HEB during neural differentiation. Although the DKO studies suggest that there is some redundancy between E2A and HEB during neural differentiation, the differences in E2A and HEB target genes in hESCs provide strong evidence that they also play independent roles in this process. Furthermore, the targeting and activity of E2A/HEB complexes are dependent on the Nodal signaling pathway, which promotes association with SMADs over PRC2. This environment is in turn dictated by the direct control of NODAL components of E2A during neural differentiation. In summary, this study highlights how E2A acts to bring context specificity to the expression of neural genes and the NODAL signaling pathway to control lineage-specific gene expression and cell fate determination during early human development.

MATERIALS AND METHODS

Cell culture

hESCs (H1; WiCell Research Institute) were maintained and expanded on plates coated with growth-factor-reduced Matrigel in serum-free, defined TeSR-E8 medium (Stemcell Technologies). Cells were passaged by non-enzymatic dissociation using 0.5 mM EDTA (Cellapy Technologies).

HEK293T cells were originally from American Type Culture Collection and were cultured in Dulbecco's modified Eagle's medium (DMEM) (Life Technologies) with 10% fetal bovine serum (Life Technologies) and antibiotics.

Development (2020) 147, dev190298. doi:10.1242/dev.190298

Generation of E2A KO hESCs

E2A KO hESCs were generated with CPRISPR-Cas9 genome editing technology. Double guide RNA plasmids targeting the genome regions of interest were bought from GenePharma Company. After transfection with Lipofectamine 3000 (Life Technologies), GFP^+ hESCs were sorted using flow cytometry. Single cells were cultured on Matrigel-coated plates in TeSR-E8 medium supplemented with Rho kinase (ROCK) inhibitor Y-27632 (Tocris Bioscience). Individual colonies were picked and expanded. Aliquots of cells were collected for purification of genomic DNA using Universal Genomic DNA kit (CWBIO). Mutations were validated by sequencing products of PCR amplification of the regions flanking the targeting sites.

Immunostaining

hESCs and neural differentiated cells were passaged on Matrigel-coated plates, and cells were cultured in TeSR-E8 medium and neural induction medium (Stemcell Technologies), respectively. Cells were fixed in 4% paraformaldehyde, and permeabilization and blocking were performed in 5% normal goat serum (Abcam) and 1% Triton X-100 (Sigma-Aldrich) in PBS for 30 min. Cells were stained with primary antibody at different dilutions. Secondary antibody was applied for 1 h at room temperature. Nuclei were stained with DAPI (Life Technologies). Images were acquired using a TCS SP8 MP FLIM confocal microscope (Leica). The antibodies used in the experiment are listed in Table S1.

Colony-forming assay and alkaline phosphatase staining

To examine self-renewal of wild-type and E2A KO hESCs, 1000 single cells were seeded per well in six-well dishes as previously described (Niwa et al., 1998). Cells were grown for 7 days and then stained with alkaline phosphatase (AP) staining kit. The numbers of colonies in each group were counted under a microscope. For AP staining, an AP detection kit (G1480; Solarbio) was used. Briefly, cells were fixed with 4% paraformaldehyde for 3-5 min followed by washing with PBS. Stain solution was applied to cover the cells at room temperature in the dark for 15-20 min. After washing the cells with PBS, images were taken.

EdU proliferation assay

In order to investigate the proliferation rate of wild-type and E2A KO cells during the neural differentiation period, wild-type and E2A KO hESCs were seeded into a confocal dish and recovered overnight. Neural induction began when the cell confluence reached 60%. After a 3 day neural induction, 100 µl EdU solution (20 µM) was added and incubated for 4 h. After 4 h, the media containing EdU were aspirated and cells were fixed with 4% paraformaldehyde for 30 min at room temperature. Next, the fixation solution was aspirated and cells were rinsed three times with PBS. After aspirating PBS, cells were permeabilized for 30 min at room temperature and rinsed twice with PBS. Finally, 100 µl EdU-488 staining mix was added to each dish and incubated for 30 min in the dark. Cells were then rinsed three times with PBS and stained with Hoechst 33342 for 10 min. Cells were visualized and counted using a TCS SP8 MP FLIM confocal microscope (Leica).

Co-immunoprecipitation and western blot analysis

Briefly, cellular lysates were prepared by incubating the cells in lysis buffer (50 mM Tris-HCl, pH 7.5, 150 mM NaCl, 0.5% NP-40, 2 mM EDTA) containing protease inhibitor cocktail (Roche) for 20 min at 4°C, followed by centrifugation at 14,000×***g*** for 15 min at 4°C. The protein concentration of the lysates was determined using BCA protein assay kit (Pierce) according to the manufacturer's protocol. Overall, 5% (1:20) cellular extracts were used for input. For immunoprecipitation, 500 µg of protein was incubated with 1 µg specific antibodies for 12 h at 4°C with constant rotation; 60 µl of 50% protein A or G agarose beads was then added and incubation was continued for an additional 2 h. Beads were then washed five times using the lysis buffer. Between washes, the beads were collected by centrifugation at 500×***g*** for 5 min at 4°C. The precipitated proteins were eluted from beads by resuspending the beads in 2×SDS-PAGE loading buffer and boiling for 10 min. The resultant materials from immunoprecipitation or cell lysates were resolved using 10% SDS-PAGE gels and transferred onto PVDF membrane (Millipore). For western blotting, membranes were incubated with appropriate antibodies for 1 h at room temperature or overnight at 4°C followed by incubation with secondary antibody. Immunoreactive bands were visualized using western blotting Luminol reagent (ThermoFisher Scientific) according to the manufacturer's recommendation.

Teratoma formation in SCID mice

All animal studies were approved by Ethics Committee of Experimental Research of Peking University and were in accordance with the International Animal Care and Use Committee Guidelines. Mice were housed under a 12 h light/dark cycle under pathogen-free conditions at 22±2°C with food and water available *ad libitum*. Six- to eight-week-old non-obese diabetic/severe combined immunodeficient (NOD/SCID) mice were injected subcutaneously with 1×10^7 hESCs resuspended in DMED-F12 with 50% Matrigel to allow teratoma formation for 8 weeks. For histology analysis, the teratoma tissue was fixed in 4% paraformaldehyde, then embedded in paraffin wax. Serial sections of 5 µm were cut and mounted on polylysine-coated slides. The sections were subjected to Hematoxylin and Eosin staining and immunohistochemical staining.

Definitive endoderm cell differentiation

To initiate definitive endoderm cell differentiation, hESCs were plated onto Matrigel-coated six-well plates at 50-60% cell confluence, and cultured in MCDB medium plus 1.5 g/L$NaHCO_3$, 4.5 mM glucose, 0.1% BSA, 1% glutamine, activin A (100 ng/ml), Wnt3a (25 ng/ml), PI103 (50 µM) and pVc (0.25 mM) for 2 days. The medium was then changed into MCDB medium plus 1.5 g/l $NaHCO_3$, 4.5 mM glucose, 0.1% BSA, 1% glutamine, activin A (100 ng/ml) and pVc (0.25 mM) for another 2 days. After 4 days of induction, the cells were collected for extracting total RNA and FACS analysis.

Hematopoietic progenitor cell differentiation via EB formation

To generate EBs, we treated hESCs with collagenase B (1 mg/ml; Roche) for 20 min. Cells were gently scraped with a cell scraper to form small aggregates (10-20 cells). Aggregates were resuspended in StemPro 34 (Invitrogen), supplemented with L-glutamine (2 mM; Gibco), ascorbic acid (1 mM; Gibco), monothioglycerol (4×10^{-4} M; Sigma-Aldrich) and transferrin (150 mg/ml; Roche). BMP4 (10 ng/ml; R&D), basic fibroblast growth factor (5 ng/ml; Peprotech), SB431542 (6 µM; Tocris), vascular endothelial growth factor (15 ng/ml; R&D), interleukin 6 (IL6) (10 ng/ml; R&D), insulin-like growth factor (25 ng/ml; R&D), IL11 (5 ng/ml; R&D) and stem cell factor (SCF) (50 ng/ml; Miltenyi) were added as indicated (Fig. 3B). Cultures were maintained in a 5% CO_2/5% O_2/90% N_2 environment. On the day of assay, EBs were harvested and dissociated into single cells by a 40 min treatment with 0.2% collagenase IV. Afterwards, 1 ml medium with serum was added and the EBs were dissociated to single cells by passaging six times through a 20-gauge needle. The FACS analysis for CD34 expression was carried out 8 days after differentiation.

Neural ectoderm cell differentiation

To initiate neural differentiation, hESC were plated onto Matrigel-coated 12-well plates at 95-100% cell confluence, and then cultured in neural induction medium (Stemcell Technologies), changing to fresh culture medium every 2 days. The cells were collected for FACS analysis, and total RNA was extracted from undifferentiated hESCs and differentiating hESCs at days 0, 3 and 6.

Flow cytometry analysis

For transcription factor detection, the cells were digested to generate single cells with Accutase (Sigma) and fixed with True-Nuclear Fix solution (Biolegend) for ∼1 h at room temperature, then washed twice with True-Nuclear Perm Buffer (Biolegend). After washing, cells were incubated with primary antibodies and isotype control antibodies for 30 min at 37°C. The cells were washed twice and resuspended in 200 µl PBS, and then analyzed using a BD Calibur (BD Biosciences). For cell surface marker detection, the cells were digested with Accutase and stained for 30 min at 4°C. The cells

Development (2020) 147, dev190298. doi:10.1242/dev.190298

were washed twice, resuspended in 200 µl PBS and analyzed with a BD Calibur (BD Biosciences). The information for antibodies is listed in Table S1.

Virus production and infection of hESCs

Lentiviral particles encoding full-length human E2A were commercially synthesized using the EF1a-GFP-Puro vector system (Genechem). hESCs were transduced with E2A and control lentivirus (Genechem), and the next day the medium was replaced with fresh TeSR-E8 medium and cultured for a further 72 h. GFP^+ cells were sorted and expanded.

Real-time qPCR

Total RNA was prepared with TRIzol (Invitrogen) and treated with RNase-free DNase (Qiagen). RNA (1 µg) was transcribed into cDNA using Oligo(dT) with Superscript III Reverse Transcriptase (Invitrogen). Real-time qPCR was performed on a 7500 Real-Time PCR System (Applied Biosystems). All experiments were carried out in triplicate using Power SYBR Green Master Mix (Applied Biosystems). Gene expression was evaluated as Delta Ct relative to GAPDH. Primer sequences are listed in Table S2.

Cell count kit 8 (CCK8) assay

When cell density reached 80%, hESCs were dissociated with Accutase to form a single cell suspension. After counting, the cells were seeded in Matrigel pre-coated 96-well with a cell density of 1.5×10^3/well. After 24, 48 and 72 h of incubation, 10% CCK8 (Dojindo) was added into the culture medium for another 2 h of incubation. The optical density values at 490 nm were measured using a microplate reader.

ChIP-seq

The ESCs and neural differentiated cells were maintained in mTeSR-E8 medium and Neural induction medium, respectively. Approximately 5×10^7 cells were used for each ChIP assay. Briefly, cross-linked and isolated nuclei were sonicated using a Diagenode Bioruptor to an average size of ~250 bp for ChIP-seq. After pre-clearing with BSA-blocked protein G Sepharose, chromatin was incubated with antibodies at 4°C overnight. The chromatin immunocomplexes were recovered with the same BSA-blocked protein G beads. For ChIP-seq library construction, ~5 ng of DNA was extracted from immunocomplexes. Libraries were prepared according to the manufacturer's instructions. In-depth whole-genome sequencing of the purified DNA library was performed by the Active Motif company. ChIP-seq samples were subjected to strict quality control by the sequencing company, and the results were obtained from a single sample. The raw sequencing data underwent quality control via the Fastx toolkit for reliable subsequent analysis with the default parameters, i.e. only sequences with at least 90% base pair with quality score >20 were retained. Remaining sequences were aligned to the unmasked human reference genome (GRGH37, hg19) using Bowtie Version 2 with only one mismatch allowed. MACS Version 2 (model-based analysis for ChIP-Seq) was used for the identification of E2A-specific binding peaks with all default settings except $q<0.05$. Genomic distribution of E2A binding sites was analyzed by ChIPseeker with hg19 genomic annotation, and 3000 bp upstream of transcription start sites were considered as promoter regions. *De novo* motif screening was performed on sequences ±400 bp from the centers of E2A-binding peaks using the MEME systems. The motifs within peaks on genes were searched through Find Motif Occurrence (FIMO) scanner. Biological process ontologies analysis was conducted based on the Database for Annotation, Visualization and Integrated Discovery (DAVID, https://david.ncifcrf.gov/).

RNA-seq and bioinformatic analysis

Total RNA was isolated from cells using TRIzol (Invitrogen) according to the manufacturer's protocol. Libraries were prepared using TruSeq Stranded Total RNA kit (Illumina), and rRNA depleted using Ribo-zero Gold rRNA beads. First-strand cDNA was generated using random primers, followed by second-strand cDNA synthesis, and adapter-ligated PCR-enriched products were used to create cDNA libraries. A single 'A' base was added and adapter-ligated, followed by purification and enrichment with PCR, to create cDNA libraries, which were sequenced for paired ends using the Illumina platform. Reads for each sample were aligned to the hg19 assembly of the human genome using the TopHat v2.1.0 and Bowtie v2.2.6 software packages. The significant gene list was uploaded to DAVID (https://david.ncifcrf.gov/) and 'Gene Functional Classification' was performed with GOTERM_BP_FAT, GOTERM_CC_FAT and GOTERM_MF_FAT databases. To gain further insight into the underlying biological themes, we used the online tool 'Investigate Gene Sets' of MSigDB (https://www.gsea-msigdb.org/gsea/msigdb/annotate.jsp) to evaluate the overlap of our differentially expressed target genes with MSigDB collections, and an estimate of the statistical significance (Subramanian et al., 2005; Liberzon et al., 2015).

Statistical analysis

Data from biological triplicate experiments are presented as mean±s.d., unless otherwise noted. Two-tailed unpaired Student's *t*-test was used for comparing two samples, unless otherwise noted. Statistical significance was considered at a value of $P<0.05$. Prism version 8.0 was used for statistical analysis. Before statistical analysis, variation within each group of data and the assumptions of the tests were checked.

Acknowledgements

We thank the members of Y.L.'s laboratory for helpful suggestions and discussions.

Competing interests

The authors declare no competing or financial interests.

Author contributions

Conceptualization: Y.L., S.Y.; Methodology: S.Y., X.H., Y.Z., S.Z.; Software: Y.Z., S.Z.; Validation: S.Y., X.H.; Formal analysis: Y.Z.; Data curation: S.Y., X.H.; Writing - original draft: S.Y.; Writing - review & editing: Y.L., S.Y., M.K.A., J.C.Z.-P., Q.L.; Supervision: Y.L.; Project administration: Y.L.; Funding acquisition: Y.L.

Funding

This work was funded by the National Key Research and Development Program of China (2018YFE0205300 and 2017YFA0104003 to Y.L.), the National Natural Science Foundation of China (31571517 to Y.L., 81870774 and 81800987 to Q.L.), the Beijing Municipal Natural Science Foundation (7192091 to Y.L.), the Canadian Institutes of Health Research (MOP82861 and PJT153058 to M.K.A.; FND-154332 to J.C.Z.-P.), the National Institutes of Health (1P01AI102853-01 to J.C.Z.P.), the Natural Sciences and Engineering Research Council of Canada (RGPIN-2014-05333 to M.K.A.) and the Krembil Foundation (J.C.Z.-P.). J.C.Z.-P. was supported by a Canada Research Chair in Developmental Immunology. Deposited in PMC for release after 12 months.

Data availability

RNA-seq data and ChIP-seq data have been deposited in GEO under accession number GSE154625.

Supplementary information

Supplementary information available online at
https://dev.biologists.org/lookup/doi/10.1242/dev.190298.supplemental

Peer review history

The peer review history is available online at
https://dev.biologists.org/lookup/doi/10.1242/dev.190298.reviewer-comments.pdf

References

Bain, G., Engel, I., Robanus Maandag, E. C., te Riele, H. P., Voland, J. R., Sharp, L. L., Chun, J., Huey, B., Pinkel, D. and Murre, C. (1997). E2A deficiency leads to abnormalities in alphabeta T-cell development and to rapid development of T-cell lymphomas. *Mol. Cell. Biol.* **17**, 4782-4791. doi:10.1128/MCB.17.8.4782

Belle, I. and Zhuang, Y. (2014). E proteins in lymphocyte development and lymphoid diseases. *Curr. Top. Dev. Biol.* **110**, 153-187. doi:10.1016/B978-0-12-405943-6.00004-X

Boyer, L. A., Lee, T. I., Cole, M. F., Johnstone, S. E., Levine, S. S., Zucker, J. P., Guenther, M. G., Kumar, R. M., Murray, H. L., Jenner, R. G. et al. (2005). Core transcriptional regulatory circuitry in human embryonic stem cells. *Cell* **122**, 947-956. doi:10.1016/j.cell.2005.08.020

Boyer, L. A., Plath, K., Zeitlinger, J., Brambrink, T., Medeiros, L. A., Lee, T. I., Levine, S. S., Wernig, M., Tajonar, A., Ray, M. K. et al. (2006). Polycomb complexes repress developmental regulators in murine embryonic stem cells. *Nature* **441**, 349-353. doi:10.1038/nature04733

de Pooter, R. F. and Kee, B. L. (2010). E proteins and the regulation of early lymphocyte development. *Immunol. Rev.* **238**, 93-109. doi:10.1111/j.1600-065X.2010.00957.x

Dias, S., Mansson, R., Gurbuxani, S., Sigvardsson, M. and Kee, B. L. (2008). E2A proteins promote development of lymphoid-primed multipotent progenitors. *Immunity* **29**, 217-227. doi:10.1016/j.immuni.2008.05.015

Duque-Afonso, J., Lin, C. H., Han, K., Wei, M. C., Feng, J., Kurzer, J. H., Schneidawind, C., Wong, S. H., Bassik, M. C. and Cleary, M. L. (2016). E2A-PBX1 remodels oncogenic signaling networks in B-cell precursor acute lymphoid leukemia. *Cancer Res.* **76**, 6937-6949. doi:10.1158/0008-5472.CAN-16-1899

Fiorenzano, A., Pascale, E., D'Aniello, C., Acampora, D., Bassalert, C., Russo, F., Andolfi, G., Biffoni, M., Francescangeli, F., Zeuner, A. et al. (2016). Cripto is essential to capture mouse epiblast stem cell and human embryonic stem cell pluripotency. *Nat. Commun.* **7**, 12589. doi:10.1038/ncomms12589

Fischer, B., Azim, K., Hurtado-Chong, A., Ramelli, S., Fernández, M. and Raineteau, O. (2014). E-proteins orchestrate the progression of neural stem cell differentiation in the postnatal forebrain. *Neural Dev.* **9**, 23. doi:10.1186/1749-8104-9-23

Flinders, C., Lam, L., Rubbi, L., Ferrari, R., Fitz-Gibbon, S., Chen, P. Y., Thompson, M., Christofk, H., Agus, D. B., Ruderman, D. et al. (2016). Epigenetic changes mediated by polycomb repressive complex 2 and E2a are associated with drug resistance in a mouse model of lymphoma. *Genome Med* **8**, 54. doi:10.1186/s13073-016-0305-0

Gepstein, L. (2002). Derivation and potential applications of human embryonic stem cells. *Circ. Res.* **91**, 866-876. doi:10.1161/01.RES.0000041435.95082.84

Huang, Z., Nie, L., Xu, M. and Sun, X. H. (2004). Notch-induced E2A degradation requires CHIP and Hsc70 as novel facilitators of ubiquitination. *Mol. Cell. Biol.* **24**, 8951-8962. doi:10.1128/MCB.24.20.8951-8962.2004

Jia, J., Dai, M. and Zhuang, Y. (2008). E proteins are required to activate germline transcription of the TCR Vbeta8.2 gene. *Eur. J. Immunol.* **38**, 2806-2820. doi:10.1002/eji.200838144

Kee, B. L. (2009). E and ID proteins branch out. *Nat. Rev. Immunol.* **9**, 175-184. doi:10.1038/nri2507

Lazorchak, A. S., Wojciechowski, J., Dai, M. and Zhuang, Y. (2006). E2A promotes the survival of precursor and mature B lymphocytes. *J. Immunol.* **177**, 2495-2504. doi:10.4049/jimmunol.177.4.2495

Li, Y., Brauer, P. M., Singh, J., Xhiku, S., Yoganathan, K., Zúñiga-Pflücker, J. C. and Anderson, M. K. (2017). Targeted Disruption of TCF12 Reveals HEB as Essential in Human Mesodermal Specification and Hematopoiesis. *Stem Cell Reports* **9**, 779-795. doi:10.1016/j.stemcr.2017.07.011

Liberzon, A., Birger, C., Thorvaldsdóttir, H., Ghandi, M., Mesirov, J. P. and Tamayo, P. (2015). The Molecular Signatures Database hallmark gene set collection. *Cell Syst* **1**, 417-425. doi:10.1016/j.cels.2015.12.004

Miyazaki, M., Miyazaki, K., Chen, K., Jin, Y., Turner, J., Moore, A. J., Saito, R., Yoshida, K., Ogawa, S., Rodewald, H. R. et al. (2017). The E-Id protein axis specifies adaptive lymphoid cell identity and suppresses thymic innate lymphoid cell development. *Immunity* **46**, 818-834.e4. doi:10.1016/j.immuni.2017.04.022

Niwa, H., Burdon, T., Chambers, I. and Smith, A. (1998). Self-renewal of pluripotent embryonic stem cells is mediated via activation of STAT3. *Genes Dev.* **12**, 2048-2060. doi:10.1101/gad.12.13.2048

Núñez-Enríquez, J. C. and Mejía-Aranguré, J. M. (2015). [Molecular biology and childhood leukemia: E2A-PBX1 and central nervous system relapse]. *Rev. Med. Inst. Mex. Seguro Soc.* **53**(Suppl 3), S236-S239.

Parisi, S., D'Andrea, D., Lago, C. T., Adamson, E. D., Persico, M. G. and Minchiotti, G. (2003). Nodal-dependent Cripto signaling promotes cardiomyogenesis and redirects the neural fate of embryonic stem cells. *J. Cell Biol.* **163**, 303-314. doi:10.1083/jcb.200303010

Pfurr, S., Chu, Y. H., Bohrer, C., Greulich, F., Beattie, R., Mammadzada, K., Hils, M., Arnold, S. J., Taylor, V., Schachtrup, K. et al. (2017). The E2A splice variant E47 regulates the differentiation of projection neurons via p57(KIP2) during cortical development. *Development* **144**, 3917-3931. doi:10.1242/dev.145698

Rao, C., Malaguti, M., Mason, J. O. and Lowell, S. (2020). The transcription factor E2A drives neural differentiation in pluripotent cells. *Development* **147**, dev184093. doi: 10.1242/dev.184093.

Reubinoff, B. E., Pera, M. F., Fong, C. Y., Trounson, A. and Bongso, A. (2000). Embryonic stem cell lines from human blastocysts: somatic differentiation in vitro. *Nat. Biotechnol.* **18**, 399-404. doi:10.1038/74447

Saini, J. S., Corneo, B., Miller, J. D., Kiehl, T. R., Wang, Q., Boles, N. C., Blenkinsop, T. A., Stern, J. H. and Temple, S. (2017). Nicotinamide ameliorates disease phenotypes in a human iPSC model of age-related macular degeneration. *Cell Stem Cell* **20**, 635-647.e7. doi:10.1016/j.stem.2016.12.015

Schier, A. F. (2003). Nodal signaling in vertebrate development. *Annu. Rev. Cell Dev. Biol.* **19**, 589-621. doi:10.1146/annurev.cellbio.19.041603.094522

Semerad, C. L., Mercer, E. M., Inlay, M. A., Weissman, I. L. and Murre, C. (2009). E2A proteins maintain the hematopoietic stem cell pool and promote the maturation of myelolymphoid and myeloerythroid progenitors. *Proc. Natl. Acad. Sci. USA* **106**, 1930-1935. doi:10.1073/pnas.0808866106

Shaw, L. A., Bélanger, S., Omilusik, K. D., Cho, S., Scott-Browne, J. P., Nance, J. P., Goulding, J., Lasorella, A., Lu, L. F., Crotty, S. et al. (2016). Id2 reinforces TH1 differentiation and inhibits E2A to repress TFH differentiation. *Nat. Immunol.* **17**, 834-843. doi:10.1038/ni.3461

Shen, M. M. (2007). Nodal signaling: developmental roles and regulation. *Development* **134**, 1023-1034. doi:10.1242/dev.000166

Singh, R. and Hansen, D. (2017). Regulation of the balance between proliferation and differentiation in germ line stem cells. *Results Probl. Cell Differ.* **59**, 31-66. doi:10.1007/978-3-319-44820-6_2

Subramanian, A., Tamayo, P., Mootha, V. K., Mukherjee, S., Ebert, B. L., Gillette, M. A., Paulovich, A., Pomeroy, S. L., Golub, T. R., Lander, E. S. et al. (2005). Gene set enrichment analysis: a knowledge-based approach for interpreting genome-wide expression profiles. *Proc. Natl. Acad. Sci. USA* **102**, 15545-15550. doi:10.1073/pnas.0506580102

Takayama, K. and Mizuguchi, H. (2017). Generation of human pluripotent stem cell-derived hepatocyte-like cells for drug toxicity screening. *Drug Metab. Pharmacokinet* **32**, 12-20. doi:10.1016/j.dmpk.2016.10.408

Thomson, J. A., Itskovitz-Eldor, J., Shapiro, S. S., Waknitz, M. A., Swiergiel, J. J., Marshall, V. S. and Jones, J. M. (1998). Embryonic stem cell lines derived from human blastocysts. *Science* **282**, 1145-1147. doi:10.1126/science.282.5391.1145

Thomson, M., Liu, S. J., Zou, L. N., Smith, Z., Meissner, A. and Ramanathan, S. (2011). Pluripotency factors in embryonic stem cells regulate differentiation into germ layers. *Cell* **145**, 875-889. doi:10.1016/j.cell.2011.05.017

Vagapova, E. R., Spirin, P. V., Lebedev, T. D. and Prassolov, V. S. (2018). The Role of TAL1 in Hematopoiesis and Leukemogenesis. *Acta Naturae* **10**, 15-23. doi:10.32607/20758251-2018-10-1-15-23

Vallier, L., Reynolds, D. and Pedersen, R. A. (2004). Nodal inhibits differentiation of human embryonic stem cells along the neuroectodermal default pathway. *Dev. Biol.* **275**, 403-421. doi:10.1016/j.ydbio.2004.08.031

Vallier, L., Mendjan, S., Brown, S., Chng, Z., Teo, A., Smithers, L. E., Trotter, M. W. B., Cho, C. H.-H., Martinez, A., Rugg-Gunn, P. et al. (2009). Activin/Nodal signalling maintains pluripotency by controlling Nanog expression. *Development* **136**, 1339-1349. doi:10.1242/dev.033951

Wang, Z., Oron, E., Nelson, B., Razis, S. and Ivanova, N. (2012). Distinct lineage specification roles for NANOG, OCT4, and SOX2 in human embryonic stem cells. *Cell Stem Cell* **10**, 440-454. doi:10.1016/j.stem.2012.02.016

Wills, A. E. and Baker, J. C. (2015). E2a is necessary for Smad2/3-dependent transcription and the direct repression of lefty during gastrulation. *Dev. Cell* **32**, 345-357. doi:10.1016/j.devcel.2014.11.034

Wöhner, M., Tagoh, H., Bilic, I., Jaritz, M., Poliakova, D. K., Fischer, M. and Busslinger, M. (2016). Molecular functions of the transcription factors E2A and E2-2 in controlling germinal center B cell and plasma cell development. *J. Exp. Med.* **213**, 1201-1221. doi:10.1084/jem.20152002

Woodcroft, M. W., Nanan, K., Thompson, P., Tyryshkin, K., Smith, S. P., Slany, R. K. and LeBrun, D. P. (2015). Retrovirus-mediated expression of E2A-PBX1 blocks lymphoid fate but permits retention of myeloid potential in early hematopoietic progenitors. *PLoS ONE* **10**, e0130495. doi:10.1371/journal.pone.0130495

Xu, W., Carr, T., Ramirez, K., McGregor, S., Sigvardsson, M. and Kee, B. L. (2013). E2A transcription factors limit expression of Gata3 to facilitate T lymphocyte lineage commitment. *Blood* **121**, 1534-1542. doi:10.1182/blood-2012-08-449447

Yoon, S. J., Wills, A. E., Chuong, E., Gupta, R. and Baker, J. C. (2011). HEB and E2A function as SMAD/FOXH1 cofactors. *Genes Dev.* **25**, 1654-1661. doi:10.1101/gad.16800511

Yoon, S. J., Foley, J. W. and Baker, J. C. (2015). HEB associates with PRC2 and SMAD2/3 to regulate developmental fates. *Nat. Commun.* **6**, 6546. doi:10.1038/ncomms7546

Zhuang, Y., Soriano, P. and Weintraub, H. (1994). The helix-loop-helix gene E2A is required for B cell formation. *Cell* **79**, 875-884. doi:10.1016/0092-8674(94)90076-0

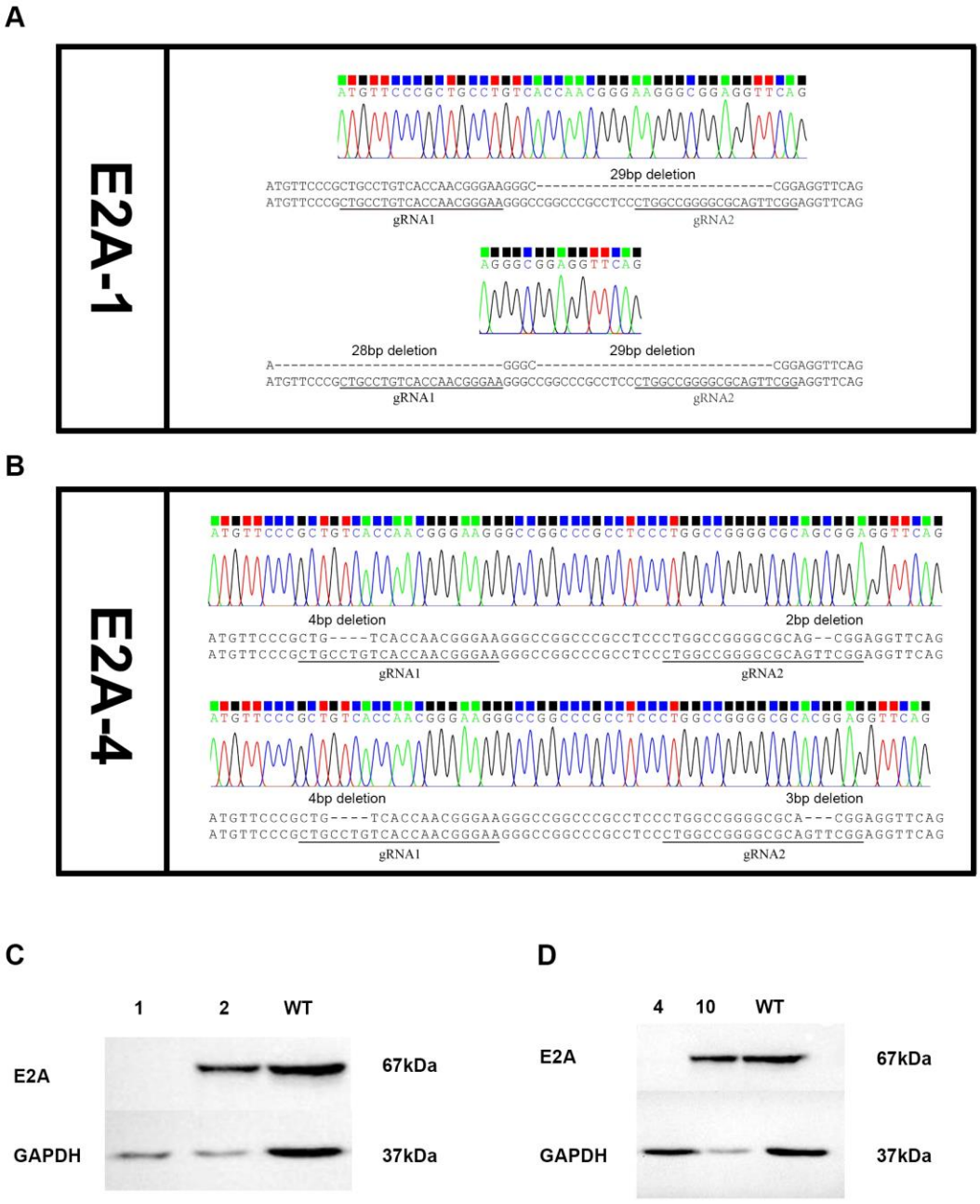

Fig. S1. Generation of E2A KO hESCs lines KO-1 and KO-4 by CRISPR-Cas9 targeting of the E2A gene locus.

A-B. Sanger sequencing of genomic DNA from two E2A KO clones (KO-1 and KO-4) comparing the sequences to WT.

C-D. Western blot analysis of E2A protein expression in wild type and E2A KO hESCs for both KO-1 and KO-4.

Images in (A), (B), (C), (D) are representative of three independent experiments.

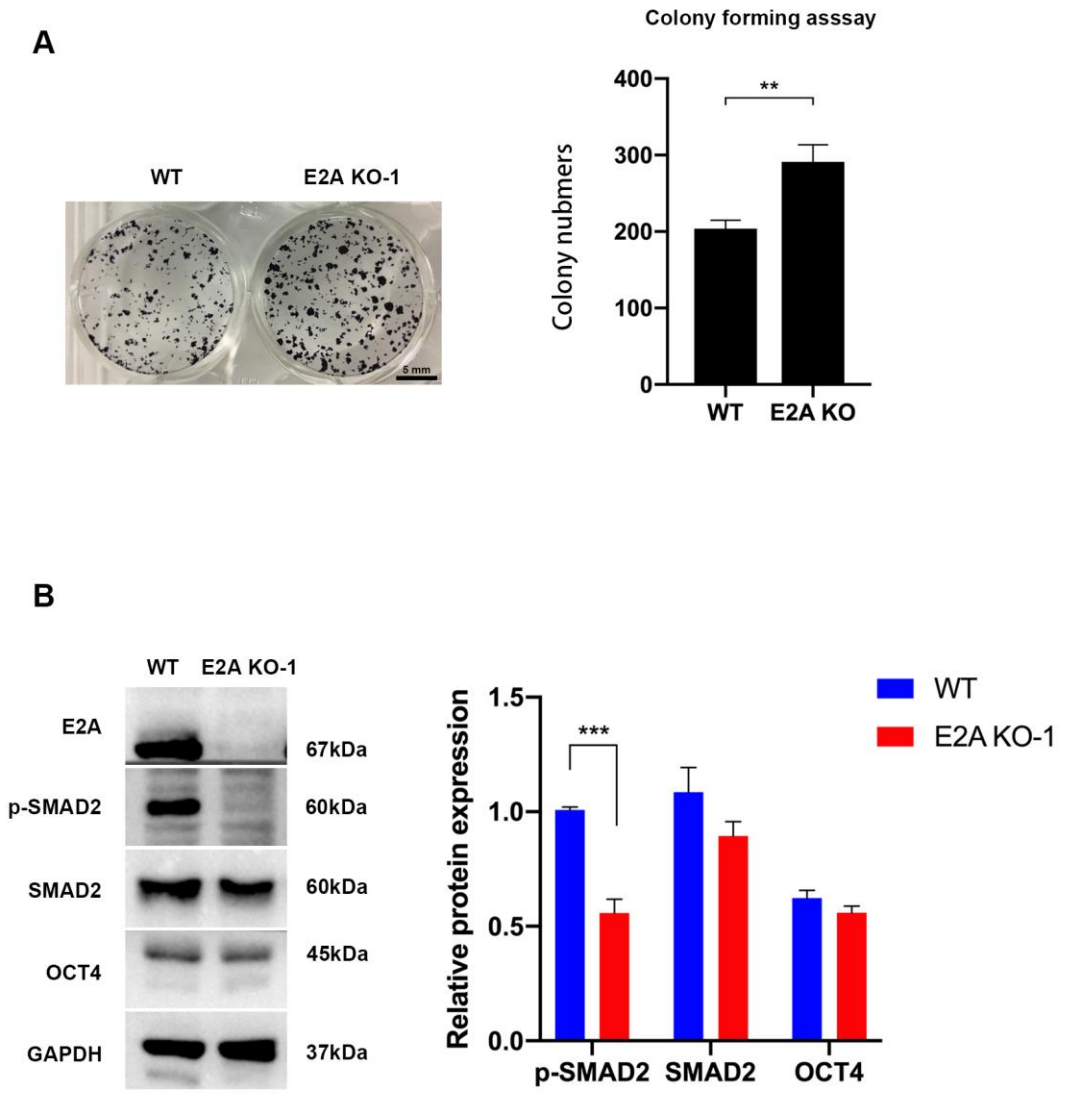

Fig. S2 Comparison of colony forming ability and nodal signalling pathway expression in WT and E2A KO hESCs.

A. Colony forming and quantitative analysis of WT and E2A KO hESCs.

B. Western blot and quantitative analysis of p-SMAD2, SMAD2 and OCT4 in WT and E2A KO hESCs.

Images and graphs in (A), (B) are representative of three independent experiments. Error bars represent mean ± SD (n = 3 independent experiments). *$p < 0.05$, ** $p < 0.01$, *** $p < 0.005$ by Student's test. Scale bars in (A) 5mm

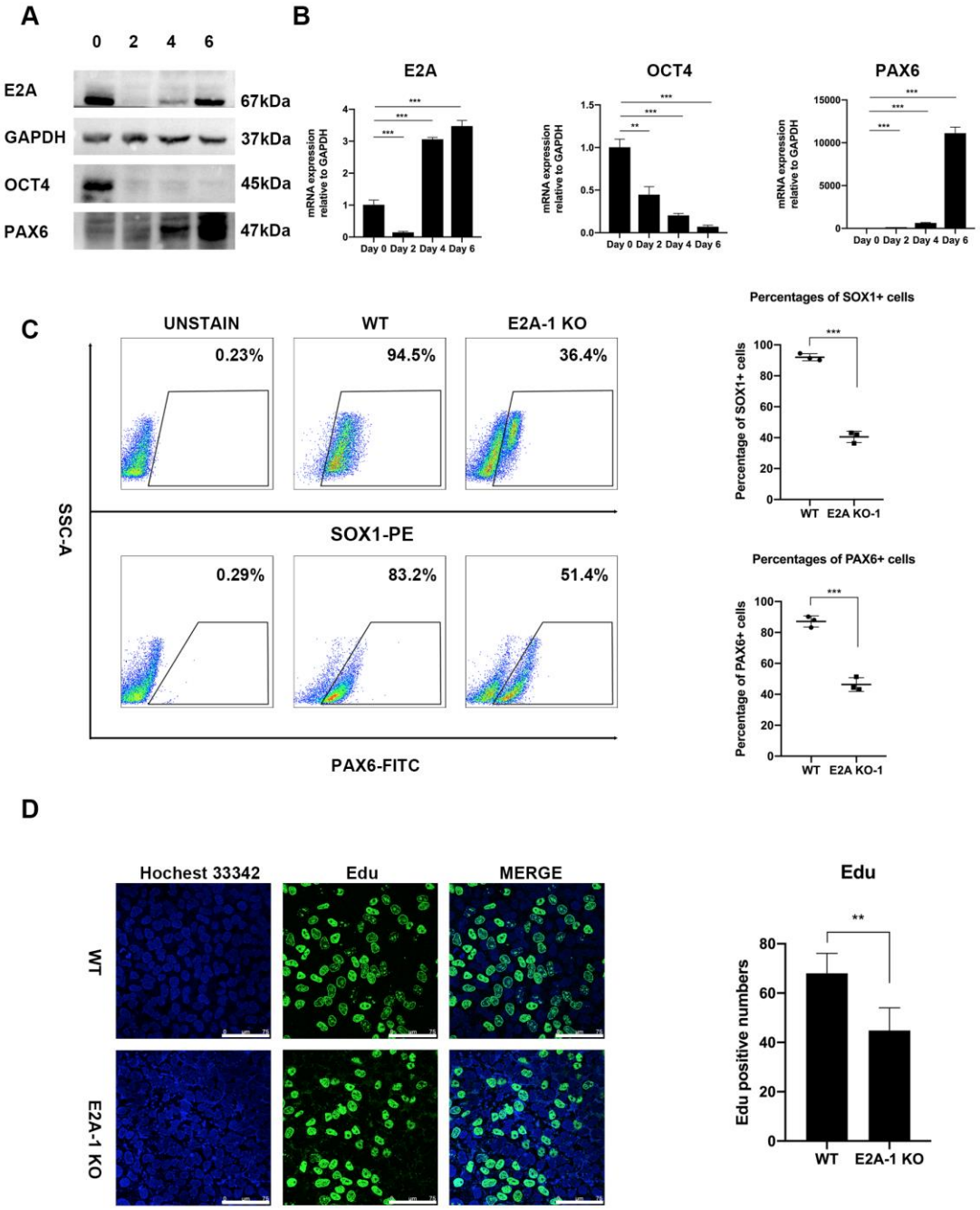

Fig. S3 The function of E2A in neural ectoderm differentiation.

A. Western blot analysis of E2A, OCT4 and PAX6 in neural induction period.

B. qPCR analysis of E2A, OCT4 and PAX6 in neural induction period.

C. Flow-cytometric analysis and percentage of SOX1 and PAX6 expression on d9 neural differentiated cells.

D. Edu staining and quantitative analysis of positive cells on neural differentiated WT and E2A KO cells.

Images in (A), (C), (D) and graphs in (B), (C), (D) are representative of three independent experiments. Error bars represent mean ± SD (n = 3 independent experiments). *$p < 0.05$, ** $p < 0.01$, *** $p < 0.005$ by Student's test. Scale bars in (D) 75um

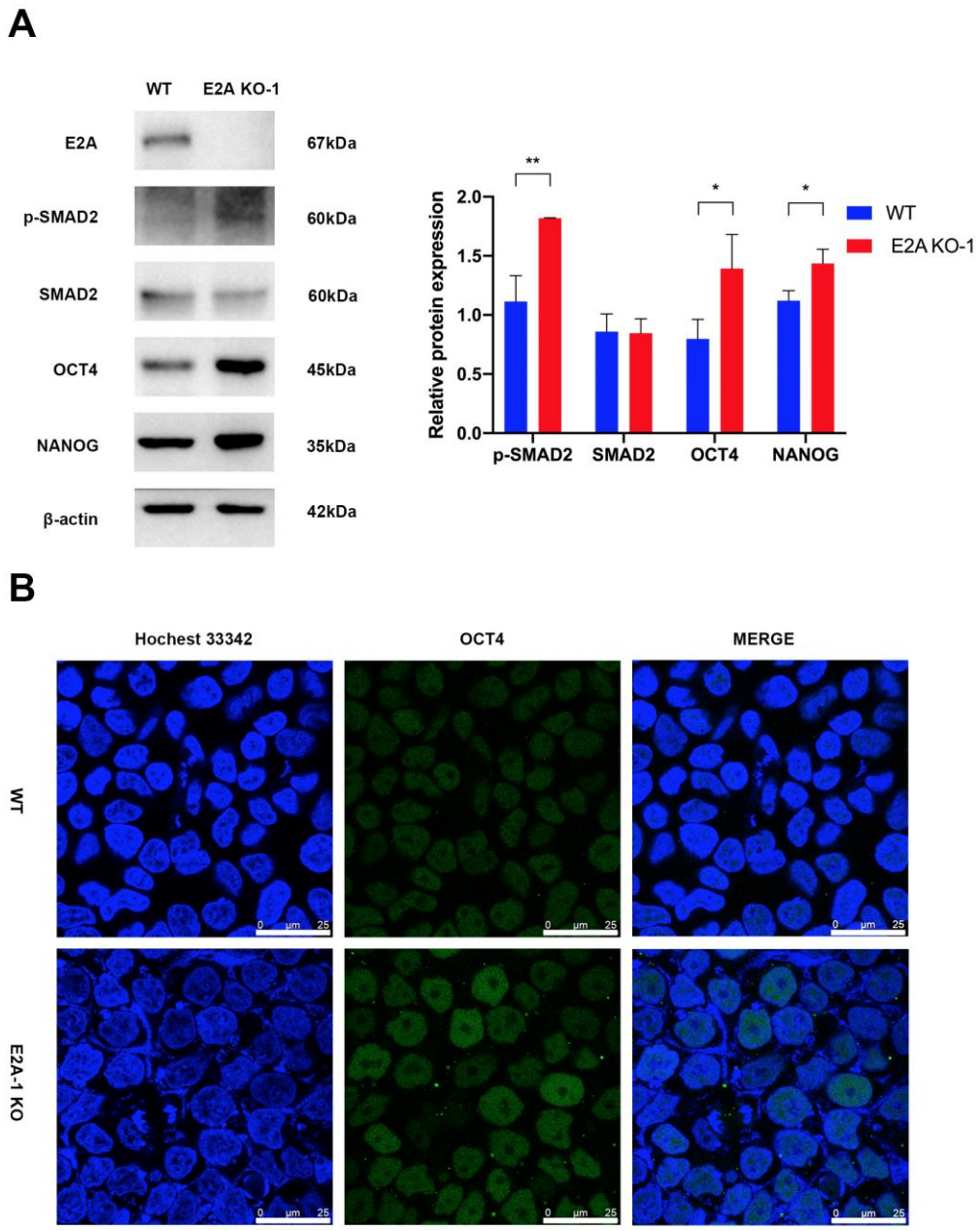

Fig. S4 The function of E2A in NODAL signaling and pluripotency markers during neural ectoderm differentiation.

A Western blot and quantitative analysis of p-SMAD2, SMAD2, OCT4 and NANOG on d3 neural differentiated cells.

B. Immunofluorescent staining of OCT4 on d3 neural differentiated cells.

Images in (A), (B) and graphs in (A) are representative of three independent experiments. Error bars represent mean ± SD (n = 3 independent experiments). *$p < 0.05$, ** $p < 0.01$ by Student's test. Scale bars in (D) 25um

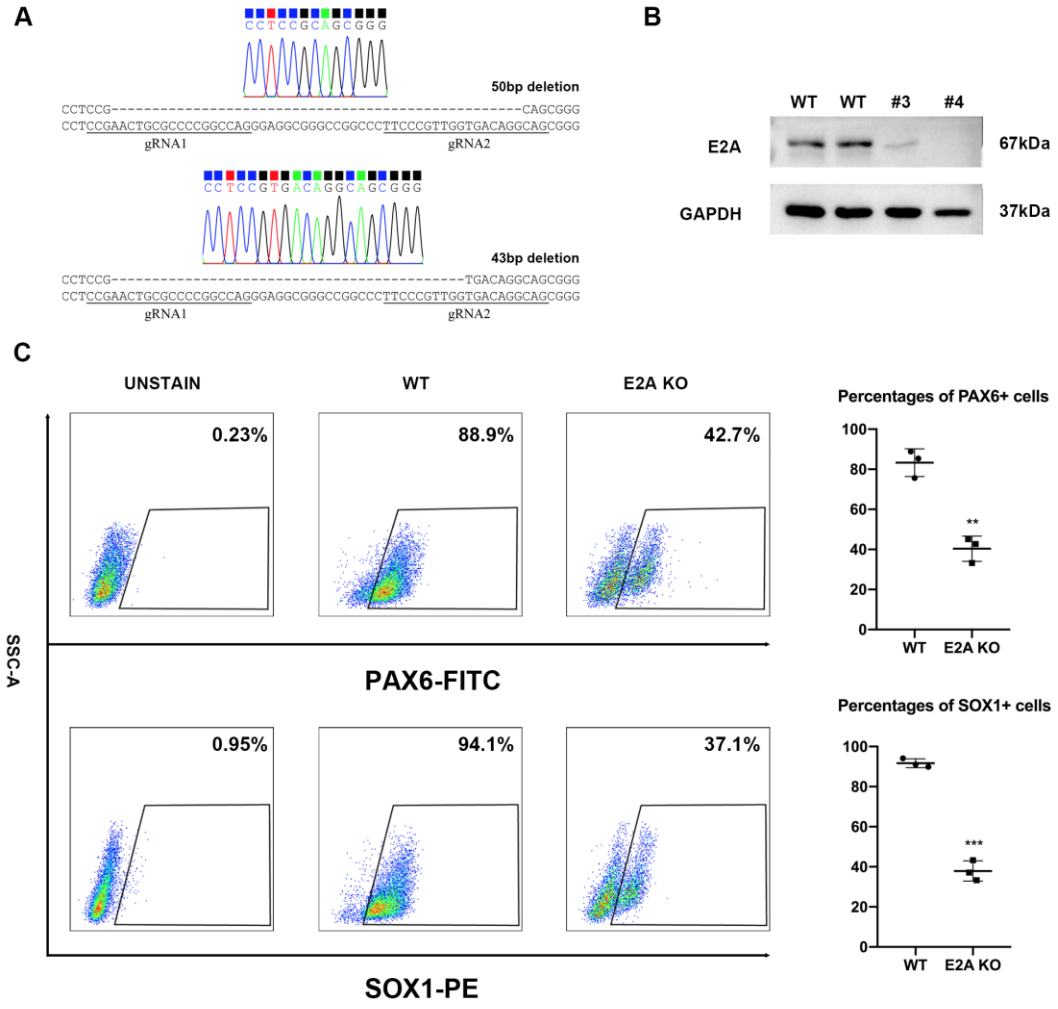

Fig. S5. A. Experimental results comparing WT and KO-4 E2A$^{-/-}$ H9 hESC line.

A. Sanger sequencing of genomic DNA from E2A KO clone (KO-4 H9) comparing the sequences to WT.

B. Western blot analysis of E2A protein expression in WT and E2A KO H9 hESCs for KO-4.

C. Flow-cytometric analysis and percentage of SOX1 and PAX6 expression on d6 neural differentiation of WT and E2A KO-4 H9 hESCs.

Images in (A), (B) and graphs in (C) are representative of three independent experiments. Error bars represent mean ± SD (n = 3 independent experiments). ** $p < 0.01$, *** $p < 0.005$ by Student's test.

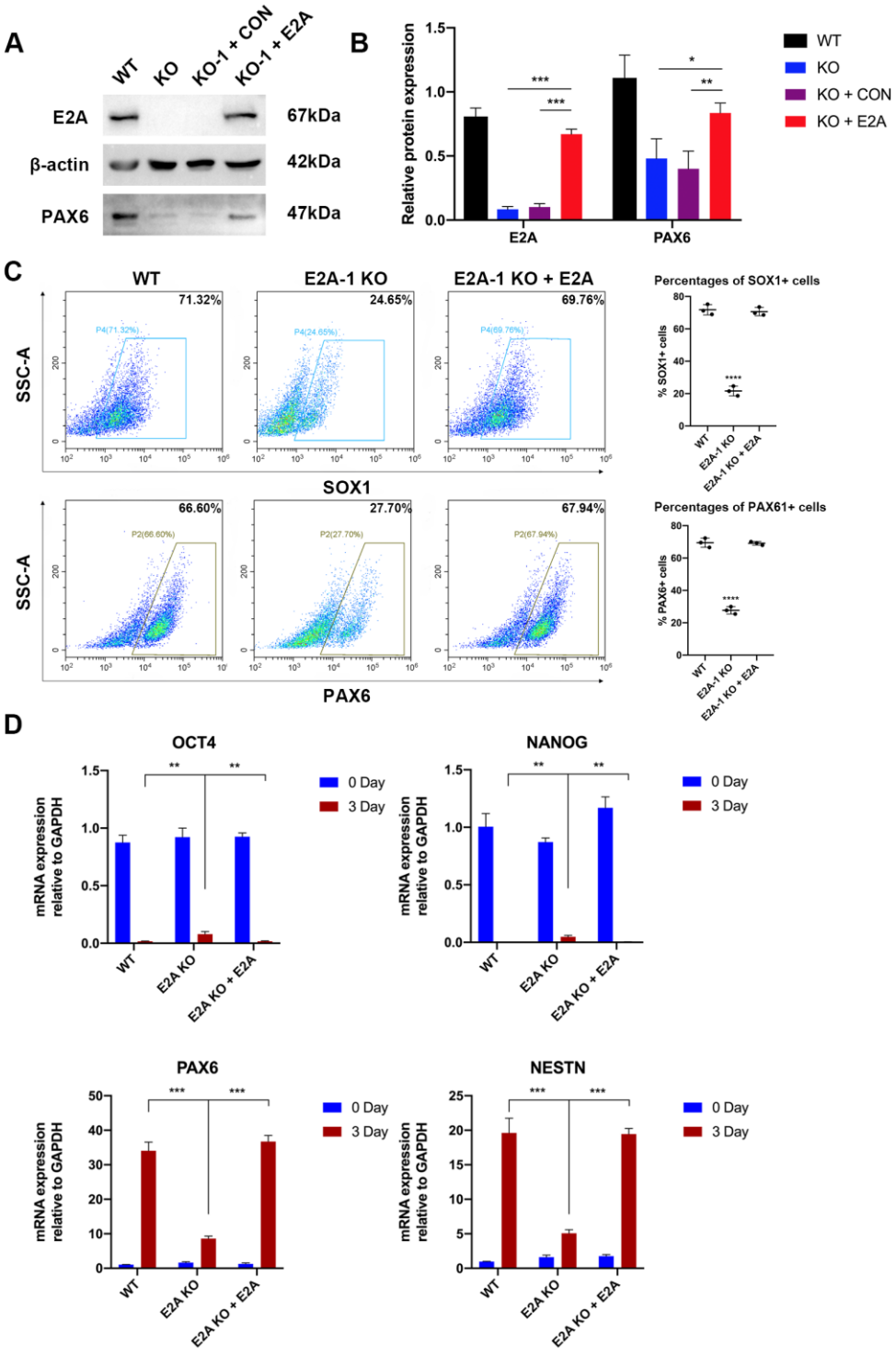

Fig. S6. Ectopic E2A rescues E2A KO hESCs neural differentiation defects.

A. Western blot analysis of E2A and PAX6 in wild type, E2A KO, E2A KO+hOE, E2A KO+ CON cells after 3 days' neural differentiation.

B. Quantitative analysis of western blot results in Fig. S6A.

C. Flow cytometric analysis the percentage of SOX1 and PAX6 positive rate in wild type, E2A KO, E2A KO+hOE cells after 3 days' neural differentiation. **** $p < 0.0001$.

D. qPCR analysis for expression of pluripotency and differentiation markers in undifferentiated hESCs (day 0) and d3 neural differentiation cells. ** $p < 0.01$, *** $p < 0.005$.

Images in (A), (B), plots in (C) and graphs in (C), (D) are representative of three independent experiments. Error bars represent mean ± SD (n = 3 biological replicates). ** $p < 0.01$, *** $p < 0.005$, **** $p < 0.0001$ by Student's test.

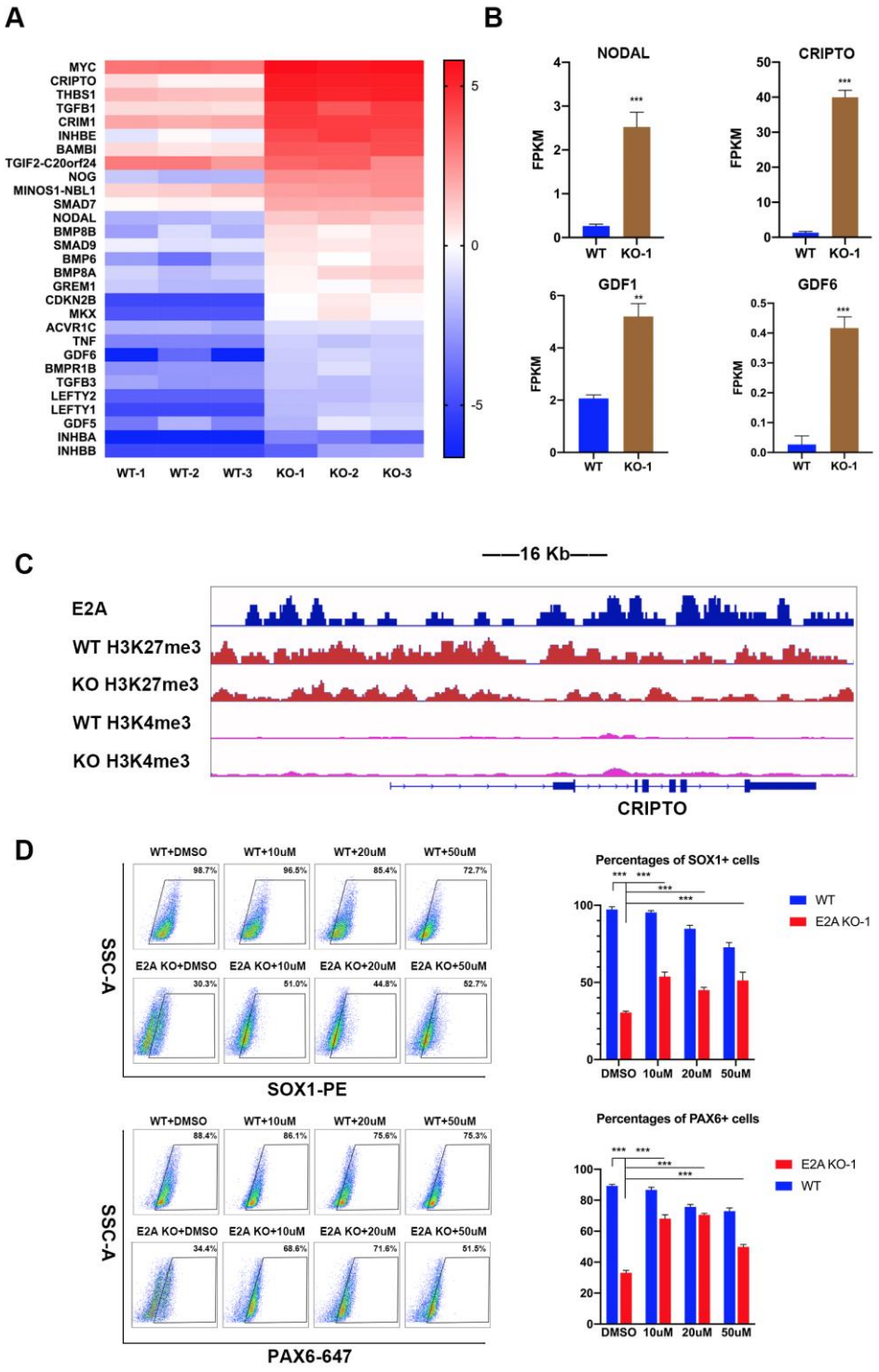

Fig. S7. SB431542 partially rescues E2A KO hESCs neural differentiation defects.

A. Heatmap of NODAL signalling related different expressing genes on d3 wild type neural differentiated cells.

B. Expression of NODAL signalling related genes after 3 days' neural differentiation, as determined by RNA-seq. FPKM, fragments per kilobase of exon per million fragments mapped.

C. The binding of E2A, H3K27me3 and H3K4me3 on NODAL signalling agonist CRIPTO.

D. Flow cytometric analysis and percentage of SOX1 and PAX6 positive expression in wild or E2A KO hESCs at day 3 after neural differentiation. The cells were treated with DMSO and SB431542 during neural differentiation.

Plots and graphs in (D) are representative of three independent experiments. Error bars represent mean ± SD (n = 3 biological replicates). * p <0.05, ** p < 0.01, *** p < 0.005 by Student's test.

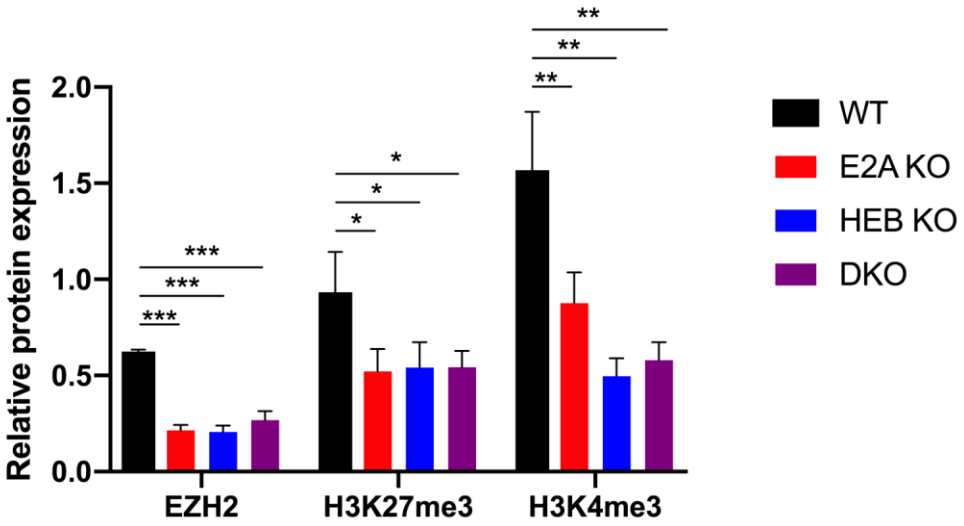

Fig. S8 Quantitative analysis of EZH2, H3K27me3 and H3K4me3 expression in Fig. 6B by image J software.

Graph in Fig. S8 are representative of three independent experiments. Error bars represent mean ± SD (n = 3 biological replicates). * p <0.05, ** p < 0.01, *** p < 0.005 by Student's test.

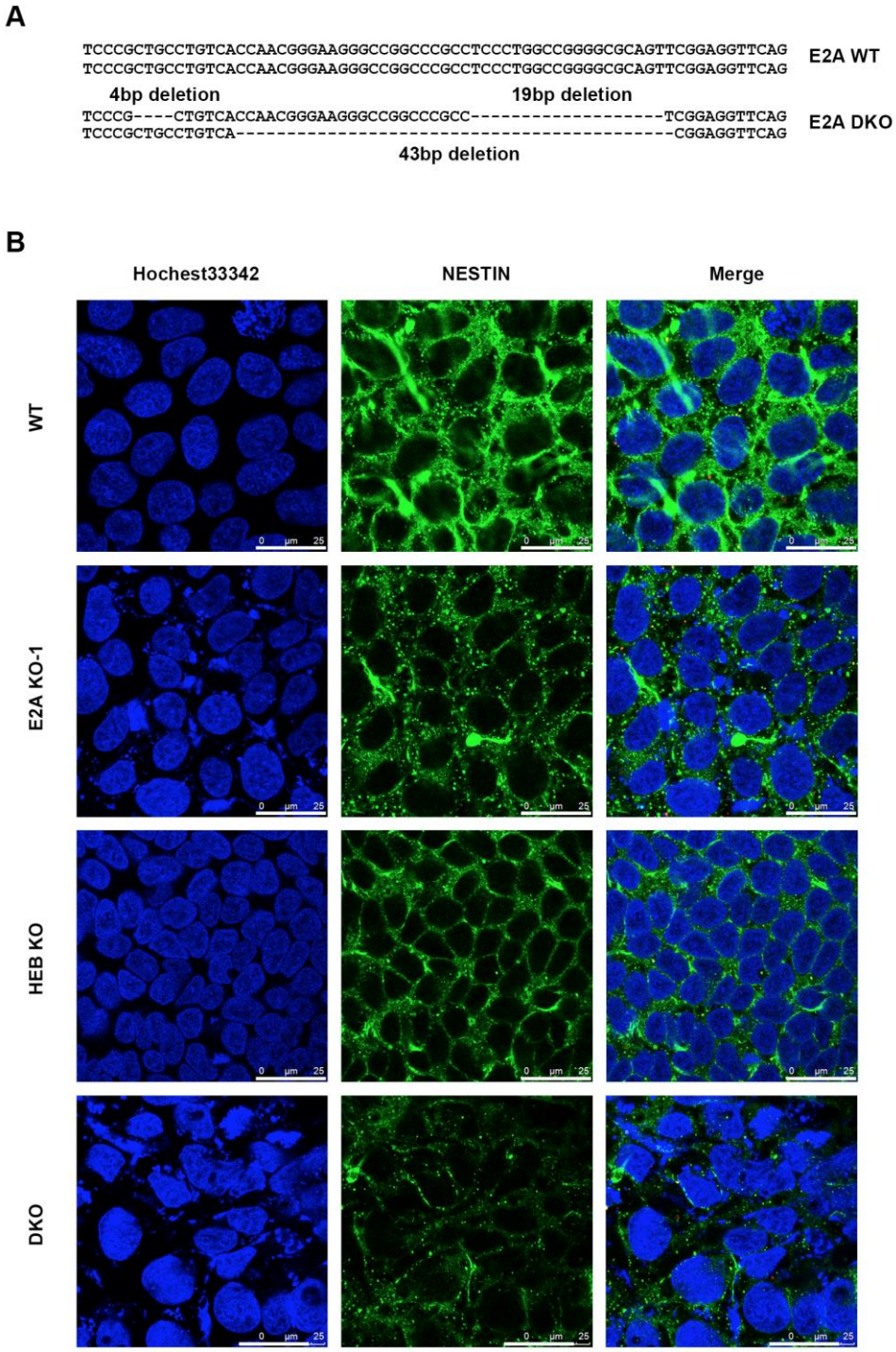

Fig. S9 E2A/HEB double knockout (DKO) hESCs display a more severe neural differentiation defects.

A. Sanger sequencing of genomic DNA from E2A/HEB double knockout cells on E2A alleles comparing the sequences to WT.

B. Immunofluorescence analysis of NESTIN in wild type, E2A KO, HEB KO, E2A KO/HEB KO double knockout (DKO) hESC after 3days' neural differentiation.

Images in (A), (B) are representative of three independent experiments. Scale bars in (D) 25um

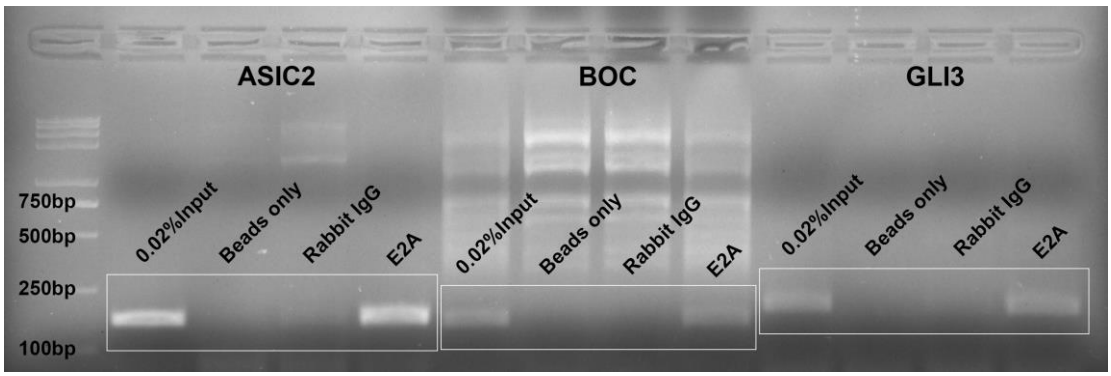

Fig. S10 The uncropped representative image of ChIP-PCR related to Fig. 5E

Images are representative of three independent experiments.

Table S1 Antibodies used in this study

Click here to Download Table S1

Table.S2 ChIP-PCR and qPCR primers used in this study

Gene	Primer forward	Primer reverse
E2A	GGCCCTGAGCCTCCGTTCTC	TCGAGGGCCG CCTCTCGCCG
T	TATGAGCCTCGAATCCACATAGT	CCTCGTTCTGATAAGCAGTCAC
MESP1	TCGAAGTGGTTCCTTGG	TGCTTGCCTCAAAGTGTC
OCT4	CTTGAATCCCGAATGGAAAGGG	GTGTATATCCCAGGGTGATCCTC
NANOG	ACAACTGGCCGAAGAATAGCA	GGTTCCCAGTCGGGTTCAC
ASIC2	AAGCCGAAGGATGTACAGAAGG	GCTGAGCCGCGCTAAA
BOC	ATCGTCACCAAAGGCCAGAG	TAGGTGCCTGAGTCCTCCTC
LEF1	TCCCGTGAAGAGCAGGCTAA	AGGCAGCTGTCATTCTTGGAC
LMX1A	GCTCAGATCCCTTCCGACAG	GAGGTGTCGTCGCTATCCAG
NRP2	TGCAGTGGACATCCCAGAAA	TTTCTTTGTCGGTCGAGGGG
GLI3	GTGAGCGAGAAAGCCGTTG	TCGTCACTCGATGTTGAAGGT
SOX2	CCGTTCATCGACGAGGCTAA	ATGTGCGCGTAACTGTCCAT
GATA4	GTGTCCCAGACGTTCTCAGTC	GGGAGACGCATAGCCTTGT
GATA6	CTGCGGGCTCTACAGCAAG	GTTGGCACAGGACAATCCAAG
SOX17	CCTTCACGTGTACTACGGCG	GTTCAAATTCCGTGCGGTCC
SOX1	CAACCAGGACCGGGTCAAAC	CCTCGGACATGACCTTCCACT
PAX6	CGAGACTGGCTCCATCAGAC	CTTTTCGCTAGCCAGGTTGC
NESTIN	AAGAGACTCAACAGCGACGG	TCTTGTCCCGCAGACTTCAG
GAPDH	TCTCCTCTGACTTCAACAGCGAC	CCCTGTTGCTGTAGCCAAATTC
ASIC2(ChIP-PCR)	ACCTGGTTTAAGCCGGACAA	CGTTGGATTTCTGGCTTCCT
BOC(ChIP-PCR)	CTCCTGGGGTTTTTGTTGATGT	CCCTCAGCATTCTCCCATCAC
GL3(ChIP-PCR)	CGTCCTGTCTGCTCCCATC	GGGGATGGCTTTGGGAAAATG

Table S3. All significant differences in gene expression between WT and E2A$^{-/-}$ hESCs as determinated by RNA-seq.

Click here to Download Table S3

Table S4. The E2A ChIP-Seq binding peaks in WT hESCs.

Click here to Download Table S4

Table S5. GO analysis of E2A ChIP-Seq in hESCs.

Click here to Download Table S5

Table S6. All significant differences in gene expression between WT and E2A$^{-/-}$ NPCs as determinated by RNA-seq.

Click here to Download Table S6

Table S7. The E2A ChIP-Seq binding peaks in WT NPCs.

Click here to Download Table S7

Table S8. GO and mSigDB analysis of E2A directly regulated genes.

Click here to Download Table S8

Table S9. H3K4me3 and H3K27me3 binding peaks in wild type and E2A^{KO} NPCs

Click here to Download Table S9

Table S10. H3K4me3 and H3K27me3 binding peaks in wild type and E2A^{KO} NPCs

Click here to Download Table S10